IMAGE: A MAP OF THE STARS OF THE ORION CONSTELLATION

Print ISSN: 2631-8474 Online ISSN: 2631-8482

JournalPreview

London Journal of Engineering Research

Volume 25 | Issue 2 | Compilation 1.0

Great Britain Journals Press

WWW.JOURNALSPRESS.COM

Journal Content
In this Issue

Great Britain Journals Press

i. Journal introduction and copyrights
ii. Featured blogs and online content
iii. Journal content
iv. Editorial Board Members

1. Analysis of Dynamic Characteristics of Straight Cylindrical Gears based on Gyroscopic Effects. ***1-14***
2. A Hybrid Multi-Attribute Framework for Optimizing Turnaround Inspection Scope in Oil and Gas Facilities. ***15-31***
3. Search of Floating Mines by Unmanned Aerial Vehicles using Kinematic Projection Methods. ***33-50***
4. Effectiveness of Silica Fume as a Partial Cement Replacement in Recycled Aggregate Concrete. ***51-59***

v. Great Britain Journals Press Membership

Analysis of Dynamic Characteristics of Straight Cylindrical Gears based on Gyroscopic Effects

Pengpeng Xu, Lifeng Chen & Mingjun Wang

Hunan University of Science and Technology

ABSTRACT

Purpose: The main objective of this study is to investigate the effect of the phenomenon of shaft plane inclination caused by bending moments and torsional vibrations during rotation on the performance of gears without considering the effect of gear tooth friction.

Methods: The law of vortex effects on gear vibrations was also considered. A four-degree-of-freedom straight-tooth cylindrical gear dynamics model was developed based on the gyroscopic effect. The finite element analysis of the model was conducted using ANSYS Workbench, with the objective of investigating the variation rule of the intrinsic characteristics of straight cylindrical gears under the action of the gyroscopic effect, and Simulink simulation analysis of the model to compare the dynamic characteristics of straight cylindrical gears, considering and not considering the gyroscopic effect.

Keywords: gyroscopic effect, straight cylindrical gears, dynamic characteristics, vortex motion, torsional vibration, translational vibration, finite element analysis, gear dynamics, frequency variation, campbell diagram.

Classification: DCC Code: 621.833

Language: English

Great Britain Journals Press

LJP Copyright ID: 392921
Print ISSN: 2631-8474
Online ISSN: 2631-8482

London Journal of Engineering Research

Volume 25 | Issue 2 | Compilation 1.0

Analysis of Dynamic Characteristics of Straight Cylindrical Gears based on Gyroscopic Effects

Pengpeng Xu[α], Lifeng Chen[σ] & Mingjun Wang[ρ]

ABSTRACT

Purpose: The main objective of this study is to investigate the effect of the phenomenon of shaft plane inclination caused by bending moments and torsional vibrations during rotation on the performance of gears without considering the effect of gear tooth friction.

Methods: The law of vortex effects on gear vibrations was also considered. A four-degree-of-freedom straight-tooth cylindrical gear dynamics model was developed based on the gyroscopic effect. The finite element analysis of the model was conducted using ANSYS Workbench, with the objective of investigating the variation rule of the intrinsic characteristics of straight cylindrical gears under the action of the gyroscopic effect, and Simulink simulation analysis of the model to compare the dynamic characteristics of straight cylindrical gears, considering and not considering the gyroscopic effect.

Results: The gyroscopic effect is the focus of current investigation, with the objective being to ascertain the variation law of the intrinsic characteristics of straight cylindrical gears. The dynamic characteristics of straight cylindrical gears with and without gyroscopic effects were compared, and the impact of gyroscopic effects on straight cylindrical gear systems was discussed. The analysis results demonstrate that, given the gyroscopic effect, the amplitude of the translational vibration displacement change of the master wheel is 14×10^{-3} mm, and the maximum magnitude of the torsional vibration displacement is 3rad. In contrast, the amplitude of the translational vibration displacement change of the follower wheel is 4×10^{-2} mm, and the maximum magnitude of the torsional vibration displacement is 1.1rad. In the absence of consideration for the gyroscopic effect, the translational vibration displacement of the master/follower wheel varies by 6×10^{-4}mm, and the maximum magnitude of the torsional vibration displacement is 0.03 rad.

Conclusions: Forward and backward vortex phenomena can be observed under the influence of the gyroscopic effect,as the intrinsic frequency increases with rotational speed. The results show that the gyroscopic effect significantly affects the translational and torsional vibrations of the master/follower wheel. Owing to the complexity of gear operating conditions or the unknown nature of certain failure mechanisms, it is necessary to investigate the dynamic characteristics of straight cylindrical gears by developing a dynamic model that takes gyroscopic effects into account during the dynamic design phase of actual gear systems, which is critical for the practice of rotor dynamics design and analysis of actual rotating machinery .

Keywords: gyroscopic effect, straight cylindrical gears, dynamic characteristics, vortex motion, torsional vibration, translational vibration, finite element analysis, gear dynamics, frequency variation, campbell diagram.

Author α ρ: College of Automotive Engineering, Xiangtan Institute of Technology, Xiangtan 411201, China.

σ: School of Mechanical Engineering, Hunan University of Science and Technology, Xiangtan 411201, China).

I. INTRODUCTION

In the context of the actual meshing process, straight-toothed cylindrical gears are not located in the centre. This is due to the presence of unevenness and other factors, as well as the gyroscopic effect. These factors result in the production of a large bending moment, which in

London Journal of Engineering Research

turn leads to nonlinear characteristics of bending and torsion vibration coupling. In the context of high-speed operation, reliance on gyroscopic torque in gears gives rise to the occurrence of vortex phenomena. At speeds approaching the critical speed, transverse vibrations emerge, consequently resulting in severe alternating loads. This, in turn, ultimately leads to fatigue failure and damage to the transmission system. Therefore, the current protocol proposes a four-degree-of-freedom dynamics model of a straight cylindrical gear based on the gyroscopic effect without considering tooth friction based on the meshing coupling dynamics model of a typical straight cylindrical gear. Considering the translational degrees of freedom and bending moments in the y-direction, as well as the rotational degrees of freedom due to torsion, simulation, and analysis of the inherent characteristics and properties are performed. The dynamic response of a straight cylindrical gear was studied using the gyroscopic effect. The simulation results are then compared with the dynamic characteristics of a straight-tooth cylindrical gear without gyroscopic effect, and the impact of the gyroscopic effect on the dynamic characteristics of straight-tooth cylindrical gears is discussed.

Although many results have been achieved in the dynamic characteristics of gears in existing research, However, the neglect of bending moments and gyroscopic effects leads to the deviation of the model from the actual working conditions. Tugan Eritenel [1–2] conducted a study on the three-dimensional non-linear vibration of a gear pair, elucidating the non-linear gear response using four parameters: the translational stiffness and torsional stiffness, acting on the centre of change of the stiffness position. The study did not take the torsional effect of bending moments into consideration, although it was founded on nonlinear gear response. O. Lundvall [3] superimposed small displacement elasticity on the rigid body motion to model the dynamics of a straight-tooth cylindrical gear. Wang Feng et al. [4] proposed a coupled bending-torsion-axis vibration model for helical gears based on the force and vibration displacement decomposition method, derived vibration differential equations for six degrees of freedom, and performed simulation calculations. Despite the establishment of a kinetic model by the studies of O. Lundvall and Wang Feng et al., the gyroscopic effect was not given full consideration. Cheng Yan-Li et al. [5] developed coupled translational-torsional dynamics model of a straight cylindrical gear with tooth surface friction. They derived vibration differential equations in six degrees of freedom in a similar study. The vibration displacement of each gear was also determined using the Runge-Kutta method, as was the dynamic meshing force of the gear pair. In a similar study, Wang Li-Hua et al. [6] developed a dynamic model of the bending-torsional-axial-torsional pendulum coupling vibration of the helical gear transmission system (comprising the helical gear, shaft and bearing). They derived the vibration differential equations with twelve degrees of freedom, calculated the vibration response of the transmission system, and performed three-dimensional finite element modal analysis. The study proposed by Zou Yu-Jing et al. [7] broadly considered the effects of time-varying meshing stiffness, bearing stiffness, and friction on dynamic behaviour. Further, a 12-degree-of-freedom helical gear friction dynamics model based on load-sharing theory and kinetic and elasto-fluid lubrication theory was developed. The tribological properties and dynamic behaviour of tooth surfaces were developed, and the coupling between them was investigated. The dynamic characteristics of gears have been well presented in all the previous studies. However, some models consider the bending moment. Only the translation in the axial direction brought by the bending moment is considered during the bending moment, and the torsion caused by the bending moment is not considered, i.e., the inclination angle deviation of the meshing plane caused by the bending moment is overlooked. Therefore, the mechanical characteristics of the gears reflected in these models are different from the actual situation and cannot fully reflect the exact movement of the gears.

The majority of extant literature pertaining to the dynamic characteristics of straight-toothed cylindrical gears concentrates on the effects of time-varying meshing stiffness, tooth surface friction and other factors on the bending-torsion-axis coupling vibration. However, the following limitations must be noted: Although part of the study considered the axial translation brought about by the bending moment, the torsional effect caused by the bending moment was ignored, i.e., the bending moment led to changes in the inclination angle of the meshing plane, which could not fully reflect the actual state of motion of the gears. At high speeds, gears generate vortex phenomena due to gyroscopic moments. However, existing studies rarely incorporate the gyroscopic effect into their models, resulting in an inability to accurately describe the dynamic characteristics of gears under high-speed rotation. Existing two-degree-of-freedom or four-degree-of-freedom vibration models do not take into account the influence of bending moments, which differ from the actual situation and cannot truly reflect the dynamic characteristics. The objective of this paper is to address the limitations of existing models in accounting for bending moment and gyroscopic effect. The present study considered the relationship between the law of vortex motion and gear vibration. A four-degree-of-freedom straight-tooth cylindrical gear dynamics model based on the gyroscopic effect is established to study the dynamic characteristics under the gyroscopic effect. Further, the dynamic characteristics of the gyroscopic effect were compared without the gyroscopic effect. Owing to the complexity of gear operating conditions or the unknown nature of specific failure mechanisms, it is necessary to investigate the dynamic characteristics of straight cylindrical gears by developing a dynamic model that takes gyroscopic effects into account during the dynamic design phase of actual gear systems, which is critical for the practice of rotor dynamics design and analysis of actual rotating machinery.

The present study improves the theoretical system of the study on the dynamic characteristics of straight-toothed cylindrical gears, provides a more accurate reference for the design and analysis of rotor dynamics of actual rotating machinery, and helps to improve the reliability and stability of the gear transmission system, and avoids fatigue failures and damages due to the inaccurate analysis of the dynamic characteristics.

II. MATERIALS AND METHODS

The gear and shaft system used in this study is made of high-strength alloy steel, a material widely used in high-speed rotating machinery for its excellent mechanical properties and wear resistance. Tables 1 and 2 list the main parameters of the gear. However, due to design, manufacturing and construction errors, the centre of mass of all actual rotors is more or less offset from the axis of rotation, resulting in dynamic imbalance of the gears. This dynamic imbalance gives rise to a deviation of the centre of mass from the two support centres, thereby triggering complex dynamic behaviour.[8] In high-speed gear shaft systems, transverse deformation of the rotating shaft occurs when it is subjected to external disturbances or its own unbalanced moments. This deformation results in a deviation of the geometric centre line of the shaft from the bearing centre line. In this case, the gear-axis system undergoes two distinct motions. Firstly, it rotates at high speed around a fixed axis, extending from the deviated axis. Secondly, the deformed rotor shaft executes a spatial slewing motion around the original static equilibrium axis. The combination of these two rotations results in the formation of the vortex phenomenon. This vortex phenomenon becomes more and more significant as the rotational speed increases, especially under high-speed operating conditions, where the gyroscopic effect further exacerbates the generation and complexity of vortices.[11] The present study proposes a mathematical model based on multi-body dynamics, the purpose of which is to facilitate a comprehensive investigation into the influence of gyroscopic effect and dynamic unbalance on the dynamic characteristics of gears. The model incorporates a series of elements, including the meshing characteristics of the gears, the elastic deformation of the rotating shaft, and the gyroscopic effect. The mass, stiffness and gyroscopic matrices of the system are obtained

through the process of discretising the gear and shaft system by means of the finite element method. It is evident that the experimental conditions imposed on the study rendered it incapable of validating the model through experimental means. However, in order to ensure the reliability and accuracy of the developed model, the theoretical correctness of the model was verified by comparing it with the classical theory.

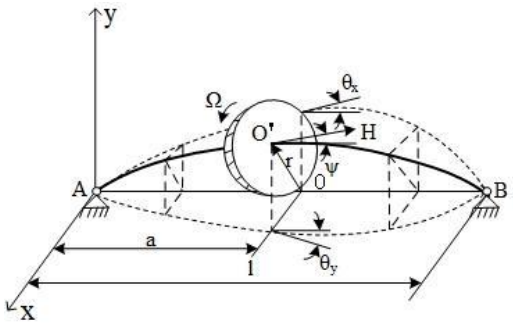

Fig. 1: Gyroscopic effect

When the disc is not mounted in the center of the two supports but is preloaded to one side, as shown in Figure 1, it is preloaded on support A. When the rotating shaft deforms during movement, the figure depicts the shaft as curved. The axis of the disc makes an angle Ψ with the line connecting supports A and B at this point.

The disk has two motions at that time: one is the rotation of the disk around its center, and the other is the rotation of the disk's center O' and the two supports A and B formed by the plane around the two-support line AB to make a circular motion which is known as the whirling motion. It is evident that, consequent to the motion, the momentum H of the disc will undergo perpetual alteration in direction, thereby engendering a moment of inertia, otherwise designated as the gyroscopic moment, which is the moment at the preloaded disc acts on the axis of rotation.

If the influence of rotating torque in the rotor structure is not significant, the difference between the intrinsic frequency and the critical speed in the modal analysis may not be significant. Nonetheless, in the context of rotor dynamics analysis, given that the gear wheels are not situated at the centre, the meshing surface is inclined at a specific angle as a consequence of the bending torque. This results in a change in the inclination angle with the bending torque, leading to a change in the mechanical characteristics; thus, it is necessary to consider the spinning torque.

As shown in Fig. 1, the gyroscopic moment is considered, and the differential equations of motion of the disc can be obtained by combining the centre of the mass theorem, as shown below [9]:

$$\{m\ddot{y} + k_{11}y + k_{14}\theta_x = 0\ m\ddot{x} + k_{22}x - k_{23}\theta_y = 0\ J_d\ddot{\theta}_y + H\dot{\theta}_x - k_{32}x + k_{33}\theta_y = 0\ J_d\ddot{\theta}_x - H\dot{\theta}_y + k_{41}y + k_{44}\theta_x = 0 \quad (1)$$

Typically, the respective stiffness coefficients have the following relationships for a single-disk rotor system with a circular cross-section of the rotor shaft .[9]

$$\{k_{11} = k_{22} = k_{rr}\ k_{33} = k_{44} = k_{\varphi\varphi}\ k_{14} = k_{41} = k_{23} = k_{32} = k_{r\varphi} = k_{\varphi r} \quad (2)$$

If the disc is mounted at the midpoint of the two supports, i.e., at a =l/2, the bending deformation equation provides the respective stiffness coefficients as follows:

$$\{k_{rr} = \frac{48EI}{l^3}\ k_{\varphi\varphi} = \frac{12EI}{l}\ k_{r\varphi} = k_{\varphi r} = 0 \tag{3}$$

Thus, the differential equation of motion for the gear considering the gyroscopic effect can be derived:

$$\{m\ddot{y} + \frac{48EI}{l^3}y = 0\ m\ddot{x} + \frac{48EI}{l^3}x = 0\ J_d\ddot{\theta}_y + H\dot{\theta}_x + \frac{12EI}{l}\theta_y = 0\ J_d\ddot{\theta}_x - H\dot{\theta}_y + \frac{12EI}{l}\theta_x = 0 \tag{4}$$

Where E is the modulus of elasticity of the material (steel); I is the cross-sectional moment of inertia of the rotating shaft; l is the span of the rotating shaft; J_d is the diameter rotational moment of inertia; H is the momentum moment of the disc.

III. MODELLING OF DYNAMICS CONSIDERING GYROSCOPIC EFFECTS

3.1 Gear Structure and Parameters

Figure 2 depicts the structure of the straight cylindrical gear used in this paper, and Tables 1 and 2 list the main parameters of the gear.

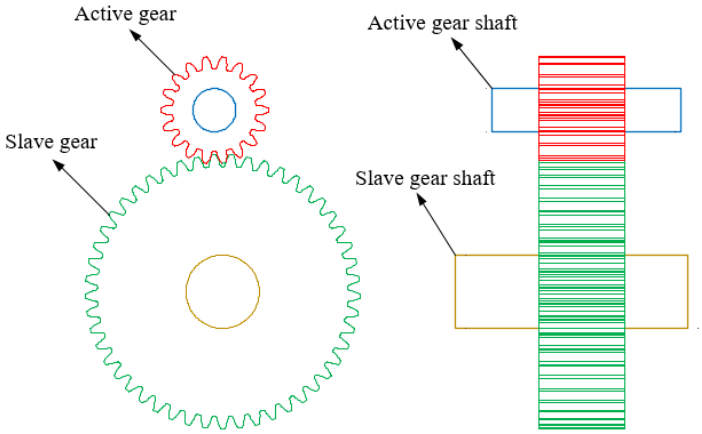

Fig. 2: Construction of Straight Cylindrical Gears

Tab. 1: Main parameters of straight cylindrical

Parameters	Active Wheel P	Slave Wheel G
Base circle radius/(m)	0.009	0.025
Mass/(kg)	0.048	0.422
Tooth number	18	49
Modulus/(mm)	1.25	
Tooth width/(m)	0.02	
Pressure angle/(°)	20	
Input torque/(N·m)	1	
Gear rotation inertia Iz/(kg·m2)	3.75e-6	2.13e-4
Engagement stiffness Km/(N·m-1)	1.57e8	
Engagement damping Cm/(N·s·m-1)	157	

Tab. 2: Main Parameters of Gear Shaft

Parameters	Active wheel P	Slave wheel G
The cross-sectional diameter of the gear shaft/(m)	0.01	0.017
Span of the gear shaft/(m)	0.044	0.054
Cross-sectional moment of inertia of gear shaft/(m4)	4.91e-10	4.1e-9
Elastic modulus/(N·m-2)	2.06e11	

3.2 Dynamical Modeling

The study describes the elasticity of the drive shaft and support bearings, but does not consider tooth friction. Furthermore, a gyroscopic effect-based dynamics model of the straight cylindrical gear was developed. The meshing coupling type dynamics model of the straight cylindrical gear pair is shown in Fig. 3.

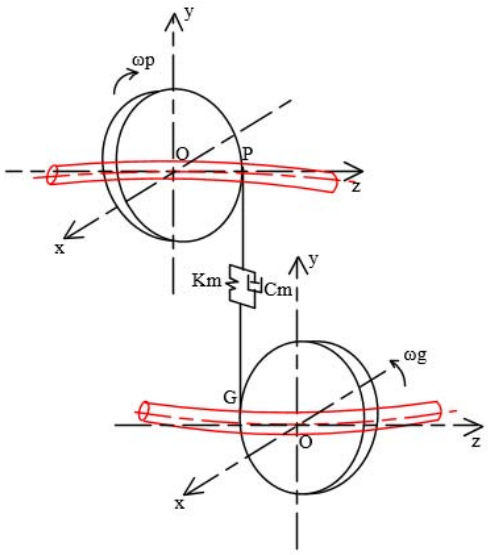

Fig. 3: Dynamics Model of Straight Cylindrical Gears

Without considering the surface friction of the gear teeth, the dynamic meshing force of the gear teeth acts in the direction of the meshing line. Consequently, the model demonstrated four degrees of freedom. The vibration displacement of these four degrees of freedom is represented by y_p, θ_p, y_g, θ_g, where y_p and y_g denote the translational vibration displacement of the central and driven wheel centre point in the y direction, and θ_p and θ_g represent the torsional vibration displacement of the central and driven wheel centre point. The generalized displacement array of the system can be expressed as follows:

$$\{\delta\} = \left\{y_p, \theta_p, y_g, \theta_g\right\}^T \tag{5}$$

Suppose the displacements of points P and G along the y-direction in Figure 2 are yp' and yg', respectively. In that case, the relationship between them and the system vibration displacement can be expressed as [10]:

$$\{y_p^{'} = y_p + R_p\theta_p \; y_g^{'} = y_g - R_g\theta_g \tag{6}$$

Further, the elastic meshing force F_k and viscous meshing force F_c between the meshing wheel teeth can be expressed as [10]:

$$F_k = k_m\left(y_p^{'} - y_g^{'}\right) = k_m(y_p + R_p\theta_p - y_g + R_g\theta_g) \tag{7}$$

and

$$F_c = c_m(\dot{y}_p' - \dot{y}_g') = c_m(\dot{y}_p + R_p\dot{\theta}_p - \dot{y}_g + R_g\dot{\theta}_g) \tag{8}$$

Km and Cm are the integrated stiffness and damping of the gear pair mesh, respectively.

Therefore, the dynamic tooth meshing forces F_p and F_g acting on the active and driven wheels can be represented:

$$F_p = F_k + F_c = -F_g \tag{9}$$

According to the above analysis, the analytical model of the system can be deduced as:

$$\{m_p\ddot{y}_p + \frac{48EI_p}{l_p^3}y_p + F_p = 0\ I_{pz}\ddot{\theta}_p + F_pR_p - T_p = 0\ m_g\ddot{y}_g + \frac{48EI_g}{l_g^3}y_g + F_g = 0\ I_{gz}\ddot{\theta}_g + T_g + F_gR_g = 0 \tag{10}$$

Where mi, I_i (i =p,g) are the masses of the primary and driven gears and the moment of inertia of the cross-section and expressed as shown below:

$$0 = m_p\ddot{y}_p + c_m\dot{y}_p + \left(k_m + \frac{48EI_p}{l_p^3}\right)y_p + c_mR_p\dot{\theta}_p + k_mR_p\theta_p - c_m\dot{y}_g - k_my_g + c_mR_g\dot{\theta}_g + k_mR_g\theta_g \tag{11}$$

$$T_p = c_mR_p\dot{y}_p + k_mR_py_p + I_{pz}\ddot{\theta}_p + c_mR_p^2\dot{\theta}_p + k_mR_p^2\theta_p - c_mR_p\dot{y}_g - k_mR_py_g + c_mR_pR_g\dot{\theta}_g + k_mR_pR_g\theta_g \tag{12}$$

$$0 = -c_m\dot{y}_p - k_my_p - c_mR_p\dot{\theta}_p - k_mR_p\theta_p + m_g\ddot{y}_g + c_m\dot{y}_g + \left(k_m + \frac{48EI_g}{l_g^3}\right)y_g - c_mR_g\dot{\theta}_g - k_mR_g\theta_g \tag{13}$$

$$-T_g = -c_mR_g\dot{y}_p - k_mR_gy_p - c_mR_pR_g\dot{\theta}_p - k_mR_pR_g\theta_p + c_mR_g\dot{y}_g + k_mR_gy_g + I_{gz}\ddot{\theta}_g - c_mR_g^2\dot{\theta}_g - k_mR_g^2\theta_g \tag{14}$$

In the matrix form, the analysis model table can be follows:

$$[m]\{\ddot{\delta}\} + [c]\{\dot{\delta}\} + [k]\{\delta\} = \{F\} \tag{15}$$

$$\{F\} = \{0\ T_p\ 0\ -T_g\}^T \tag{16}$$

$$[\boldsymbol{m}] = \begin{bmatrix} m_p & & & \\ & I_{pz} & & \\ & & m_g & \\ & & & I_{gz} \end{bmatrix} \tag{17}$$

$$[c]=\begin{bmatrix} c_m c_m R_p & -c_m c_m R_g c_m R_p c_m R_p^2 & -c_m R_p c_m R_p R_g & -c_m & -c_m R_p c_m & -c_m R_g & -c_m R_g & -c_m R_p R_g c_m R_g & -c_m R_g^2 \end{bmatrix} \quad (18)$$

$$[k]=\begin{bmatrix} k_m+\frac{48EI_p}{l_p^3} k_m R_p & -k_m k_m R_g k_m R_p k_m R_p^2 & -k_m R_p k_m R_p R_g & -k_m & -k_m R_p k_m+\frac{48EI_g}{l_g^3} & -k_m R_g & -k_m R_g & -k_m R_p R_g k_m R_g & -k_m R_g^2 \end{bmatrix} \quad (19)$$

IV. RESULTS AND DISCUSSION

4.1 Inherent Characteristics

In order to solve the finite element model of straight-toothed cylindrical gears, it is necessary to take into account the gyroscopic effect. The gyroscopic effect is defined as an inertia effect that arises from the conservation of angular momentum of a rotating object. This effect is indicative of the influence of the angular velocity of the rotating parts on the dynamics of the system, and thus plays an instrumental role in the analysis of rotating systems. Within the ANSYS Workbench, the gyroscopic effect is realised through the incorporation of the gyro matrix, which is then subjected to analysis via the Campbell plot. In ANSYS Workbench, the finite element model of a straight-toothed cylindrical gear focuses on the effect of its mass distribution on the dynamic characteristics by simplifying the gear to a mass (Point Mass), while the gear shaft is simulated using a higher-order beam cell (e.g., BEAM 188 or BEAM 189) to efficiently capture the bending and torsional deformation characteristics of the shaft. In the process of mesh generation, the mesh density is optimised according to the geometry of the axes and the stress distribution. This ensures sufficient mesh accuracy in critical areas. The boundary conditions are defined as simple support constraints at both extremities of the gear shaft. This type of constraint has been demonstrated to be superior in simulating the support conditions in actual engineering scenarios and reflecting the dynamic characteristics of the shaft system. The mass distribution of the system as a whole is primarily concentrated in the gear component, and the mass and moment of inertia of the gear are simulated by Point Mass. In the course of the simulation process, the aim is to simplify the model and enhance the computational efficiency.

In order to achieve this, the following assumptions are made:

- The gear and shaft materials are taken to be uniform isotropic materials.
- In the preliminary analysis, the friction and lubrication effects in the gear meshing process are not taken into account.

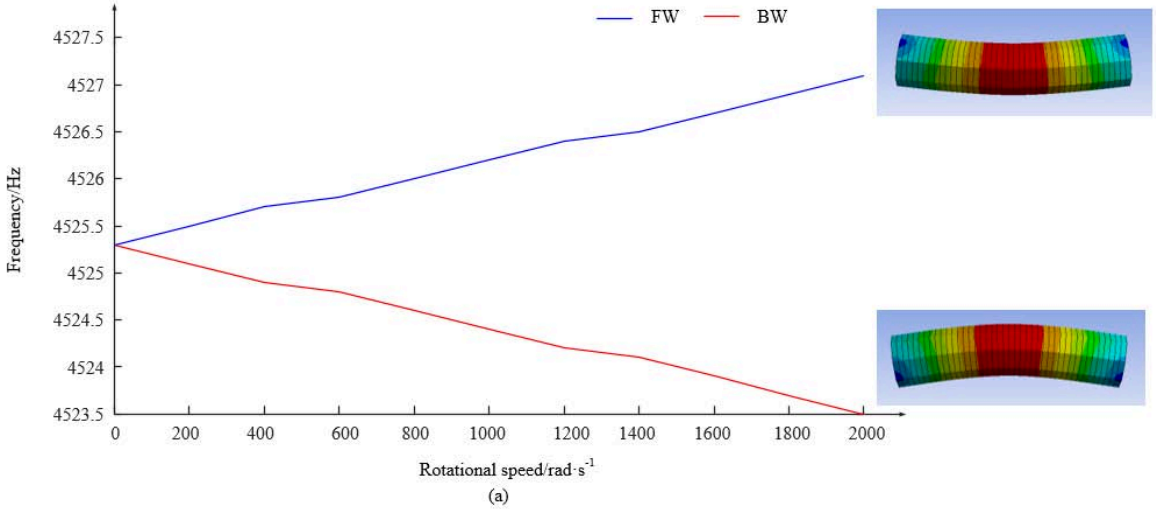

(a)

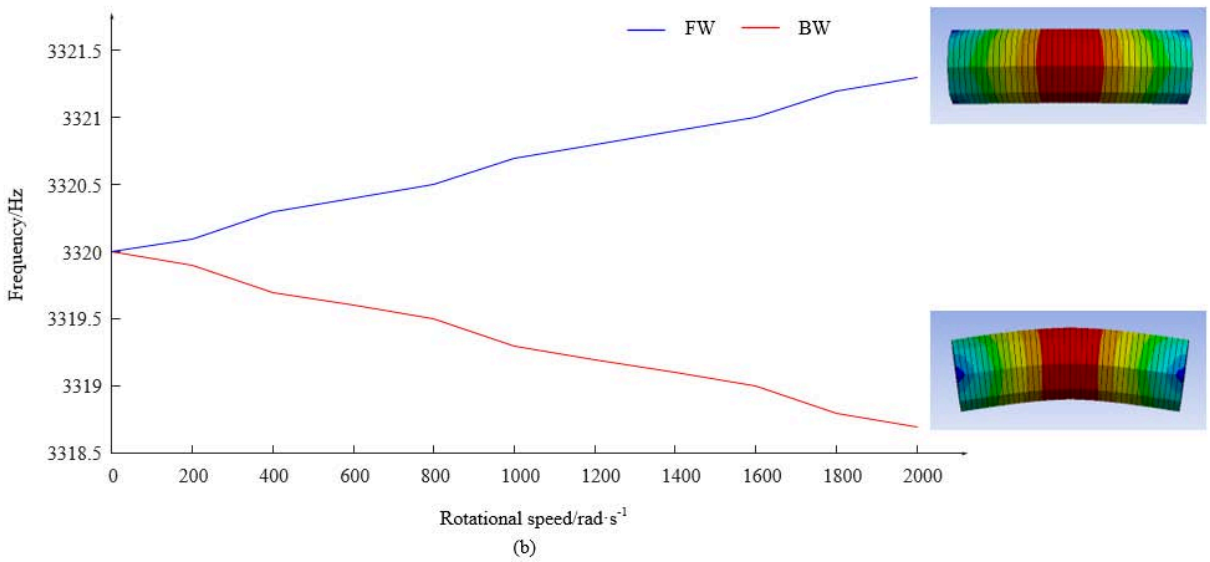

Fig. 4: Campbell Diagram of Active and Slave Gear

The results of the Campbell diagram calculations for the master and driven wheels are shown in Figure 4. The Campbell diagram for the active wheel P is displayed in Figure 4(a), and the Campbell diagram for the slave wheel G is displayed in Figure 4(b). The inherent frequency increases with speed in the figure, and the phenomenon of the forward and backward vortices can be seen, as the shaft of the high-speed gear has a rotationally symmetrical structure. When the rotational speed is 0, there are only two types of oscillations with different phases of the same inherent frequency order. The gyroscopic effect produces a reverse vortex frequency below the intrinsic frequency of the structure and a forward vortex frequency above the intrinsic frequency of the structure as the shaft rotates. The higher the velocity, the more pronounced the bifurcation.

4.2 Dynamic Response

Simulink simulation of a straight cylindrical gear dynamics model using the straight cylindrical gear parameters shown in Table 1. The time-varying meshing stiffness was replaced with the equivalent meshing stiffness. The model was created using a set of equations (10), which includes 13 known variables and 4 unknown variables. The subsystem module was used to construct the subsystems of equations (11) to (14) and the known variables connected to the four constructed subsystems via signal lines. The subsystem solution was integrated using the continuous integration module, and equation (15) was derived. By setting the simulation computation time to 10s, ode45 (Runge-Kutta) was chosen as the solver for iterative integration. As shown in Figure 5, the structural diagram of the straight cylindrical gear Simulink simulation model was created following the above steps.

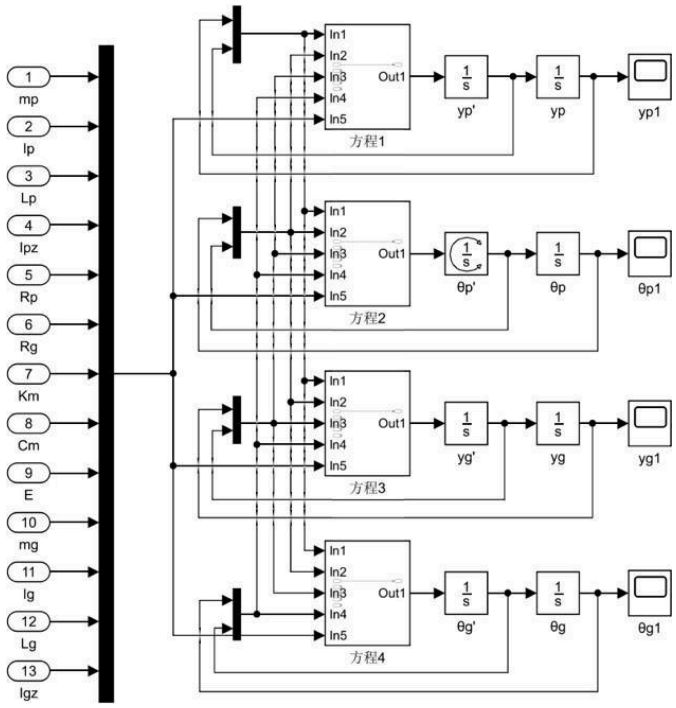

Fig. 5: Structural diagram of Simulink simulation model of spur gear

The dynamic characteristics of straight tooth cylindrical gears with and without gyroscopic effect are compared and analyzed, and the simulation results are shown in Figs. 6 to 9.

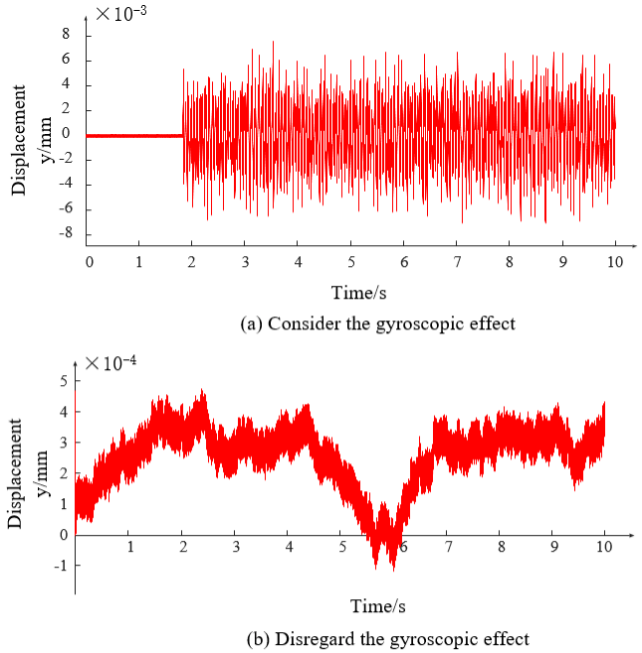

Fig. 6: Variation curve of active wheel translational vibration displacement with time

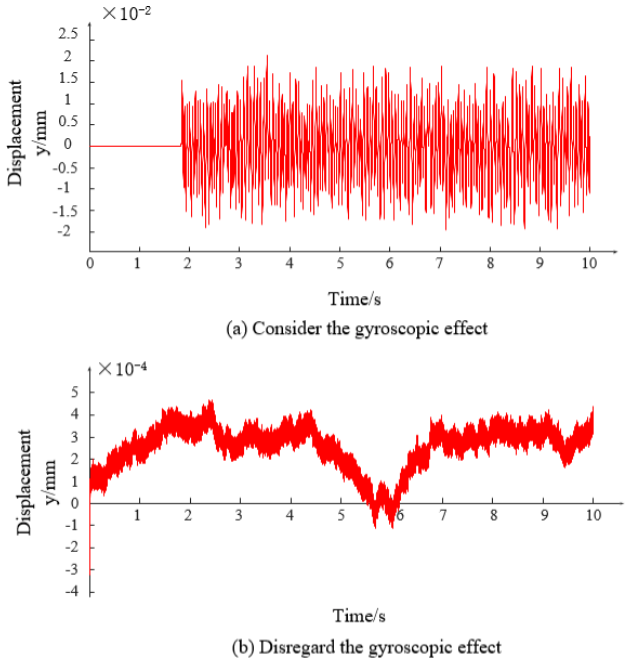

Fig. 7: Variation Curve of Slave Wheel Translational Vibration Displacement with Time

Fig. 6 represents the variation curves of the translational vibration displacement of the active wheel with time. In contrast, Fig. 7 shows the variation curves of the translational vibration displacement of the driven wheel with time. Figs. 6(a) and 7(a) illustrate the waveforms of translational vibration displacement considering the gyroscopic effect. Figs. 6(b) and 7(b) show the waveforms of translational vibration displacement without the gyroscopic effect.

It is possible to comprehend the influence of gyroscopic effects on the translational vibrational displacement of the system by comparing Figures 6(a) and 6(b). In Fig. 6(a), the translational vibration displacement of the gear remained relatively constant in the vibration amplitude during the first 2s of simulation time. The vibration amplitude increased significantly after the system worked for 2s, with a change of 14×10^{-3} mm. However, the fluctuation of the vibration amplitude was relatively smooth. In Fig. 6(b), the translational vibration displacement of the gear varied in the range of -1×10^{-4} mm to 5×10^{-4} mm with a variation of 6×10^{-4} mm.

Although the translational vibration displacement of the gear appeared small in the system without the gyroscopic effect, the fluctuations in vibration amplitude are more prominent.

The comparison of Figs. 6(a) and 7(a) shows that the amplitude of the master/follower wheel's translational vibration displacement does not change significantly during the first 2 sec of simulation time. However, after 2 s of system operation, the translational vibration displacement of the master wheel changed in the range of -6×10^{-3} mm to 8×10^{-3} mm with a variation of 14×10^{-3} mm. The translational vibration displacement of the driven wheel varied from -2×10^{-2} mm to 2×10^{-2} mm with a variation of 4×10^{-2} mm. The result revealed that the gyroscopic effect greatly influenced the translational vibration displacement of the driven wheel.

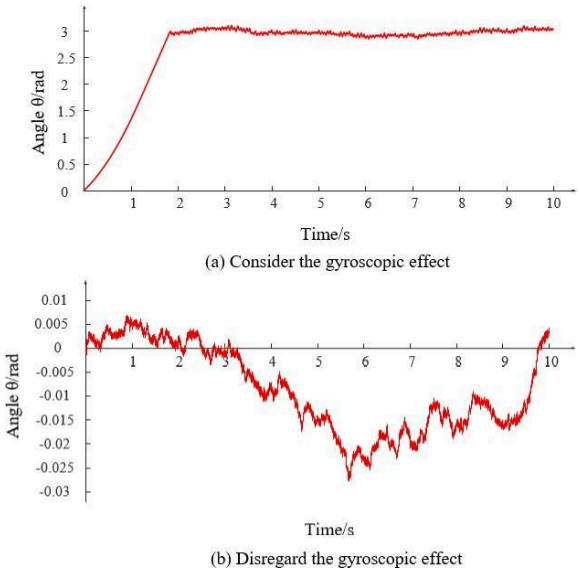

Fig. 8: Variation Curve of Active Wheel Torsional Vibration Displacement with Time

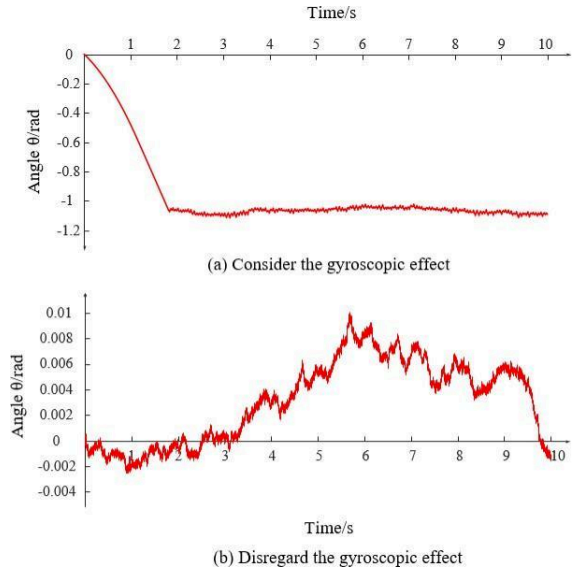

Fig. 9: Variation Curve of Slave Wheel Torsional Vibration Displacement with Time

Fig. 8 shows the variation curve of the torsional vibration displacement of the active wheel with time, and Fig. 9 shows the variation curve of the torsional vibration displacement of the driven wheel with time. Figs. 8(a) and 9(a) depict the waveforms of torsional vibration displacement considering the gyroscopic effect. In contrast, Figs. 8(b) and 9(b) show the waveforms of torsional vibration displacement without considering the gyroscopic effect.

The comparison of Figs. 8(a) and 8(b) demonstrate the gyroscopic effect on the torsional vibration displacement of the system. In Fig. 8(a), the torsional vibration displacement of the gear rises rapidly in the first 2s of simulation time, and the vibration amplitude tends to stabilize after 2s of system operation. The displacement of the vibration varies between 3 rad. The torsional vibration displacement of the gear varied from −0.03 rad to 0.01 rad with a variation of 0.04 rad, as shown in Fig. 8(b). Although the amplitude of the torsional vibration displacement of the gear is small in the absence of the gyroscopic effects, the fluctuations in the vibration amplitude was more pronounced.

The comparison of Figs. 8(a) and 9(a) further reveal that the torsional vibration bits of the master/follower wheel changed linearly and

rapidly during the first 2 s of simulation time. After 2 s of system operation, the torsional vibration displacement of the master wheel fluctuated up and down around 3 rad. Notably, the torsional vibration displacement of the follower wheel fluctuated up and down around 1.1 rad. The result suggests that the gyroscopic effect significantly impacts the torsional vibration displacement of the active wheel.

Since the rotor vortex motion is caused by the dynamic deformation of the rotor shaft, the rotor shaft will change from static deformation to dynamic deformation at some point during the gear rotation. The static deformation is minimal and the gear motion's effect is negligible. It can therefore be deduced that the gyroscopic effect is only affected following two seconds of system operation.

V. CONCLUSION

In this study, a four-degree-of-freedom straight cylindrical gear dynamics model based on the gyroscopic effect is established, and the influence law of the gyroscopic effect on the gear vibration is analysed. The analysis showed that, when the gyroscopic effect was considered, the amplitude of the translational vibration displacement change of the master wheel is 14×10^{-3} mm, and the maximum magnitude of the torsional vibration displacement is 3rad. In contrast, the amplitude of the translational vibration displacement change of the follower wheel is 4×10^{-2} mm, and the maximum magnitude of the torsional vibration displacement is 1.1 rad. In the absence of consideration for the gyroscopic effect, the translational vibration displacement of the master/follower wheel varies by 6×10-4mm, and the maximum magnitude of the torsional vibration displacement is 0.03 rad. The results show that the gyroscopic effect has a significant effect on the transverse and torsional vibrations of gears, a finding of great importance for the study of gear dynamics. In practice, understanding the mechanism of the gyroscopic effect helps to optimise gear design, improve gear life and reduce vibration, thus improving the overall performance of the mechanical system. For example, in a high-speed rotating gear transmission system, consideration of the gyroscopic effect can more accurately predict the dynamic behaviour of the gears, thereby optimising the structural parameters and operating conditions of the gears, reducing vibration and noise, and improving the reliability and efficiency of the system.

However, there are some limitations to this study. For example, the model made simplifying assumptions about the material properties and contact conditions of the gears and did not consider the effect of lubrication conditions on the dynamic characteristics. In addition, studies have mainly focused on straight cylindrical gears, and the influence of gyroscopic effects on other types of gears, such as helical cylindrical gears or bevel gears, has not yet been addressed.

Future research can be carried out in the following aspects: firstly, the model can be further improved to take into account more actual working condition factors, such as lubrication and tooth wear, in order to improve the accuracy and applicability of the model; secondly, the object of research is extended to study the difference in dynamic characteristics of different types of gears under the influence of gyroscopic effect; thirdly, in combination with experimental verification, the theoretical model and design method are further optimised by comparative analysis of actual test data and numerical simulation results.

Author Contributions

Conceptualization, Lifeng Chen; Resources, Mingjun Wang; Writing and Editing, Pengpeng Xu.; Review Lifeng Chen.; Funding Acquisition, Pengpeng Xu.

Funding

A Project Supported by Scientific Research Fund of Xiangtan Institute of Technology (2023YB23)

Conflicts of Interest

The authors declare no conflict of interest.

REFERENCES

1. Tugan Eritenel, Robert G. Parker. An investigation of tooth mesh nonlinearity and partial contact loss in gear pairs using a lumped-parameter model. 2012, 56:28–51.

2. Tugan Eritenel, Robert G. Parker. Three-dimensional non-linear vibration of gear pairs. 2012, 331(15):3628–3648.
3. O. Lundvall, N. Strömberg, A. Klarbring. A flexible multi -body approach for frictional contact in spur gears. 2003, 278(3):479–499.
4. WANG Feng, FANG Zongde, LI Shengjin. Treatment and contrast verification of meshing stiffness in dynamic model of helical gear [J]. Journal of Vibration and Shock, 2014, 33(06):13–17.
5. CHENG Yanli, XIAO Zhengming, WANG Xu. Investigation on dynamic characteristic of cylinder gears and simulation based on ADAMS [J]. Journal of Mechanical Strength, 2016, 38(04):667–674.
6. WANG Lihua, LI runFang, LIN Tengjiao, et al. Coupled vibration analysis of helical gear transmission [J]. Machine Design and Research, 2002(05):30–31+40–7.
7. ZOU Yujing, PANG Feng, FAN Zhimin. Coupling research on dynamical behavior and elastohydrodynamic lubrication property of helical gear [J]. Journal of Mechanical Engineering, 2019, 55(03):109–119.
8. SUN Huer, SU Fei, CHEN Yong, et al. Based on the gyroscopic effect of the rotor dynamic imbalance lateral-axial coupling vibration analysis [J]. Journal of Mechanical Strength, 2014, 36(03):325–329.
9. ZHONG Yie, HE Yanzong, WANG Zheng. Rotor dynamics [M]. Beijing: Tsinghua University Press, 1987:12–17.
10. LI Runfang, WANG Jianjun. Dynamics of Gear Systems - Vibration, Shock, Noise [M]. Beijing: Science Press, 1997:162–166.
11. CHENG Hao, ZHANG Aiqiang, NI De, et al. Analysis of High-Speed Gear Shafting Vortex Phenomenon and Critical Speed Considering Gyroscopic Effect [J/OL]. Mechanical Science and Technology for Aerospace Engineering, 2023:1–8.

A Hybrid Multi-Attribute Framework for Optimizing Turnaround Inspection Scope in Oil and Gas Facilities

Dr. Mohamed Attia

ABSTRACT

Purpose: The purpose of this paper is to support operating facilities in identifying the appropriate and adequate initial turnaround (TA) inspection scope strategies and prioritizing operation, maintenance & engineering efforts to help deliver production operational targets by limiting the TA on to the equipment that internal inspection is necessary and avoid unnecessary replacement of internal parts (e.g., catalysts, desiccant, etc.) due to exposing the equipment to internal inspection. Furthermore, identify the inspections that can be performed non-intrusively and online, which can shorten the TA duration, minimize business interruption, and maximize plant availability.

Design/methodology/approach: The case study was conducted using one of the most widely deployed risk models in the oil and gas industry, where a full assessment was performed on an offshore gas-producing platform.

Keywords: risk, maintenance, integrity, inspection, probability, consequence, asset, management, turnaround, refinery, planning paper type: technical paper.

Classification: LCC Code: TP692

Language: English

Great Britain Journals Press

LJP Copyright ID: 392922
Print ISSN: 2631-8474
Online ISSN: 2631-8482

London Journal of Engineering Research

Volume 25 | Issue 2 | Compilation 1.0

A Hybrid Multi-Attribute Framework for Optimizing Turnaround Inspection Scope in Oil and Gas Facilities

Dr. Mohamed Attia

ABSTRACT

Purpose: The purpose of this paper is to support operating facilities in identifying the appropriate and adequate initial turnaround (TA) inspection scope strategies and prioritizing operation, maintenance & engineering efforts to help deliver production operational targets by limiting the TA on to the equipment that internal inspection is necessary and avoid unnecessary replacement of internal parts (e.g., catalysts, desiccant, etc.) due to exposing the equipment to internal inspection. Furthermore, identify the inspections that can be performed non-intrusively and online, which can shorten the TA duration, minimize business interruption, and maximize plant availability.

Design/methodology/approach: The case study was conducted using one of the most widely deployed risk models in the oil and gas industry, where a full assessment was performed on an offshore gas-producing platform.

Findings: The newly developed methodology was implemented in various process units of newly constructed refineries. It has successfully supported the organization in developing a cost-effective I-TA scope. These use cases resulted in approximately an average 50% reduction in the original TA inspection scope and a reduction of around 30% in the TA duration. This minimizes business interruption costs, reduces the risk of cost overrun and schedule delays, ensures personnel safety, and minimizes environmental impact, i.e., Green TA.

Research limitations/implications: The presented methodology does not cover equipment and components related to control and protection, or the following installations and equipment: Fire Protection and Safety equipment and installation, Fire water, and Fire and Gas Detectors.

Originality/value: This work presents a structured framework for determining a cost-effective inspection strategy that provides satisfactory confidence in the equipment's safe and reliable operation. Developing this cost-effective TA scope is a complex process that involves considerations of a broad spectrum of issues. Therefore, the framework presented in this paper introduces a novel hybrid methodology that combines the Multi-Attribute Decision-Making (MADM) technique with Multi-Dimensional Risk Analysis (MDRA).

Keywords: risk, maintenance, integrity, inspection, probability, consequence, asset, management, turnaround, refinery, planning
paper type: technical paper.

Author: Central Engineering Services, Saudi Aramco, Dhahran, KSA.

I. INTRODUCTION

In the chemical industry, major losses are primarily generated by asset failures [18]. Therefore, adopting proper maintenance strategies allows for increased reliability while reducing the impact of unexpected breakdowns [19]. The only way to ensure the integrity and sustainability of the physical assets used in the process industries, including the oil and gas industry, is to perform turnaround (TA) maintenance with project management considerations [5]. However, in an intensely competitive global market characterized by increasing scales of production, the effective planning and management of that maintenance

activity is coming to be seen as an ever more critical business process [1]. Nowadays, TA projects have to meet very challenging safety, environmental, operability, quality, and even community affairs standards in addition to best-in-class cost and schedule goals. Consequently, a more serious and focused effort has recently gone into the design of technologies capable of monitoring and maintaining plants online, minimizing costly outages with all their attendant risks to safety, reliability, business, and the environment. While the quest for production without regular plant shutdown goes on, and the goal remains tantalizingly out of reach, there will remain the need to organize and perform significant maintenance activity in the form of plant TAs.

For static equipment, inspections play a pivotal role in ensuring integrity and reliability. If there are effective integrity management systems, most equipment failures do not occur without any warning signs [2]. However, there will remain some inspection work that can only be conducted when the plant has been taken offline and made safe for the performance of such work. Thereby, TA is defined as periodic maintenance in which plants are shutdown to allow for inspections, repairs, replacements, and overhauls that can be conducted only when the assets (plant facilities) are taken out of service [26]. TA activities typically include:

1. Work that cannot be done unless the whole plant is shutdown;
2. Work that can be done while equipment is in operation but requires a lengthy period of maintenance work and a large number of maintenance personnel; and
3. Defects that are pointed out during operation but cannot be repaired will be maintained during the TA period.

TA cost, duration, and execution strategy are dependent upon the inspection scope of work. Approximately 50% of all shutdown projects are delayed by more than 20% and 80% overrun budget by more than 10% [25]; therefore, having optimal TA scope is highly critical to the success of the TA maintenance projects. Consequently, over the past few decades, a lot was work has been done [12, 13, 14] to develop Risk-based maintenance strategies to provide a basis not only for considering the reliability of a system when making decisions regarding the type and the time for maintenance actions, but also to be able to take into consideration the risk that would result as a consequence of an unexpected failure. Furthermore, the maintenance evolved to more sophisticated strategies like condition monitoring and reliability-centered Maintenance [10]. ASME introduced a risk-based approach to manage maintenance. This is part of the holistic asset integrity management system [11]. Many research studies have highlighted the integrated and hybrid solution for maintenance decision-making, but the integration of cost, risk, and performance is something that can be researched in the future scope of work [15].

In mathematical terms, this issue of maintenance optimization or planning constitutes a sequential decision-making problem in an uncertain environment, and its resolution is a difficult challenge, and the selection of the most cost-efficient strategy is seldom straightforward. [20]. It entails using stochastic models to describe and quantify reliability, random degradation processes, or the outcome of maintenance decisions [21, 22]. The purpose of maintenance optimization is to plan preventive actions in order to get the best possible outcome according to some selected criteria, usually expected cost [20]. The process of determining the TA scope is affected by many factors and a multitude of variables, which may be stochastic, fuzzy, or unknown, and requires a comprehensive formal framework for decision making. Therefore, the motivation of this article is to establish a correlation between achieving effective TA while optimizing the maintenance and inspection resources [1].

1.1 Statement and Objectives of the Framework Proposed

TA maintenance is the most expensive maintenance activity because of the high direct cost of tools, materials, and labor, and more importantly, the indirect cost of lost revenue due

to the shutting down of production. Both cost components are directly dependent on the duration of the shutdown interval. The industry's TA performance statistics show that there is still significant improvement required to achieve predictably competitive TA results. To satisfy the present-day business environment of optimistic targets, business viability and manufacturing competitiveness are now highly defined by the ability to deliver superior TA performance.

Competitive TA performance is not possible without an aggressive scope control and optimization effort. [7] Proposed a critical index for deciding on activities that should be included in the TA process. They compared this method with the risk-based decision-making method in the case study of TA in a refinery in Italy and reported a significant improvement in resource consumption reduction. Therefore, the primary objective in planning TA maintenance activities is to minimize the length of the shutdown time duration. Other important objectives include minimizing the total cost and maximizing safety and reliability [8].

The goal of the framework presented here is to create an optimal inspection strategy that minimizes overall costs consisting of both breakdown and inspection costs. Solving multi-criteria problems like optimization can be done either by using deductive logic with scaled assumptions, or the other method is developing a hierarchy or network system and inserting all possible factors to derive all possible outcomes [23].

This paper aims to introduce a structured and logical methodology for developing a TA inspection scope that is economically justifiable with minimum risk to the enterprise.

The very first question is, 'Is the initial Turnaround necessary at all?

Performing the initial TA after the plant startup at an interval shorter than the normal or subsequent TA is recognized as a mandatory requirement in the Oil and Gas (O&G) industries to verify the design and operation integrity of the equipment for corrosion, fouling, fabrication and construction defects, and/or any other potential damage mechanisms. This is to establish baseline data and determine the subsequent TA intervals. The initial TA intends to reduce operational, health, and safety risks while capturing the following, but not limited to:

- Shortcomings inherited from design, procurement, installation, and commissioning.
- Development of inspection baselines and integrity performance records.
- Addresses Project quality deficiency carryovers.
- Ramification of equipment with improper material selection and design.
- Resolving commissioning and operational upsets.

The details of the inspection scope and the practice of inspection test planning are key variables that must be clearly defined to establish a complete and effective TA scope of work. The inspection of static equipment commenced with internal inspections to verify the equipment's mechanical integrity. This internal inspection involves taking the equipment out of service and preparing it for examination, which includes performing an internal visual inspection supported by Non-Destructive Testing (NDT).
It is worthwhile to introduce the so-named Risk-Based Shutdown (RBS), which is a particular kind of Risk-Based Inspection (RBI) or maintenance that considers the devices that cannot be maintained or inspected without stopping the operation of the plant. During the past decades, RBS has also gained much popularity in several application fields [3]. Inspection and maintenance activities are prioritized based on quantified risks resulting from equipment failure so that the overall risk of the system is minimized [9].

II. FRAMEWORK METHODOLOGY

The purpose of this work is to provide a structured framework for conducting an I-TA inspection scope optimization study, which aims to determine a cost-effective inspection strategy that provides satisfactory confidence in the equipment's safe and reliable operation. The proposed methodology aims to balance defining

and evaluating various aspects of equipment technical integrity with the necessary depth of analysis for each relevant point. This approach is intended to make cost-effective decisions while maintaining asset integrity and meeting the objectives of the initial TA. It involves examining the equipment journey from a comprehensive perspective, considering past experiences, current factors, and potential future issues.

A key characteristic of multi-attribute decision-making (MADM) problems, such as developing TA scope, is that there is typically a limited number of predetermined alternatives that correspond to varying levels of achieving the attributes. Based on these attributes, a final decision must be made. This task is quite complex and demands consideration of a wide spectrum of issues; therefore, the approach presented here seeks to add clarity and consistency to the process of identifying the most cost-effective initial TA inspection scope for every piece of equipment. It provides structured guidelines for systematically identifying and classifying the main assets' criticality while considering operational and maintenance constraints, thereby minimizing subjectivity in determining the TA scope.

The Analytic Hierarchy Process (AHP) is an MADM technique that has become, over the past decades, a very common tool for decision-making [24]. The methodology is developed based on the hierarchical model created according to AHP rules [16,17]. AHP is a robust and flexible methodology that consists of three steps: Step I, formulating the decision problem in a hierarchical structure where the top level reflects the ultimate objective of the decision problem, i.e., the optimum TA scope that balances between integrity and resources utilization. The lower layers comprise the attributes and factors that influence the decision. In the second step, the multidisciplinary team evaluates all those different attributes and their relative weights and importance, simultaneously performing multidimensional risk analysis. The team needs to agree on the preferences to incorporate subjectivity, e.g., uncertainty, biases, knowledge, augmentation of various conflicting experts' opinions, etc. The last step is determining the inspection scope based on the multidimensional (MD) risk analysis.

MCDM accounted for diverse factors that serve as central elements in determining the I-TA scope. A comprehensive review is to be conducted for the units included in the study, where the following 5 Dimensions, as illustrated in Figure 1, shall be covered:

1. Technical risk, including the operational risk, FMEA/FMECA, and residual risk from the fabrication, installation, and construction phases, and the adherent operational risk.
2. Mechanical Integrity, including startup, baseline inspection, DNs, trips, MOC, etc.
3. Historical Operation Data, i.e., sister plant/equipment inspection, maintenance, and industry practices.
4. Operation Integrity to cover compliance with integrity operating windows (IOWs), KPIs, CMP, etc.
5. Detection capability of non-intrusive inspection (NII)

Traditionally, inspecting static equipment required taking it out of service for internal visual inspection and Non-Destructive Testing (NDT). Advances in NDT now allow inspections without downtime, known as Non-Intrusive Inspection (NII). NII can enable performing inspection while the equipment is online, thereby eliminating the need for personnel to enter confined spaces to perform the inspection. This advantage can significantly decrease the frequency of confined space entries, minimizing line breaks and subsequent leak tests. Additionally, it increases equipment availability, reduces lost and deferred production, and shortens TA duration. It is estimated that as much as 80% of equipment can be assessed using non-intrusive methods [32].

However, NII must be thorough enough to identify potential damage and evaluate equipment integrity. It must also provide information for safe operation until the next turnaround. When using NII, it is crucial to show that the method is as effective as internal inspections. This part of MCDM assesses NII in verifying design integrity, applicability, capabilities, and operational limitations of online inspections.

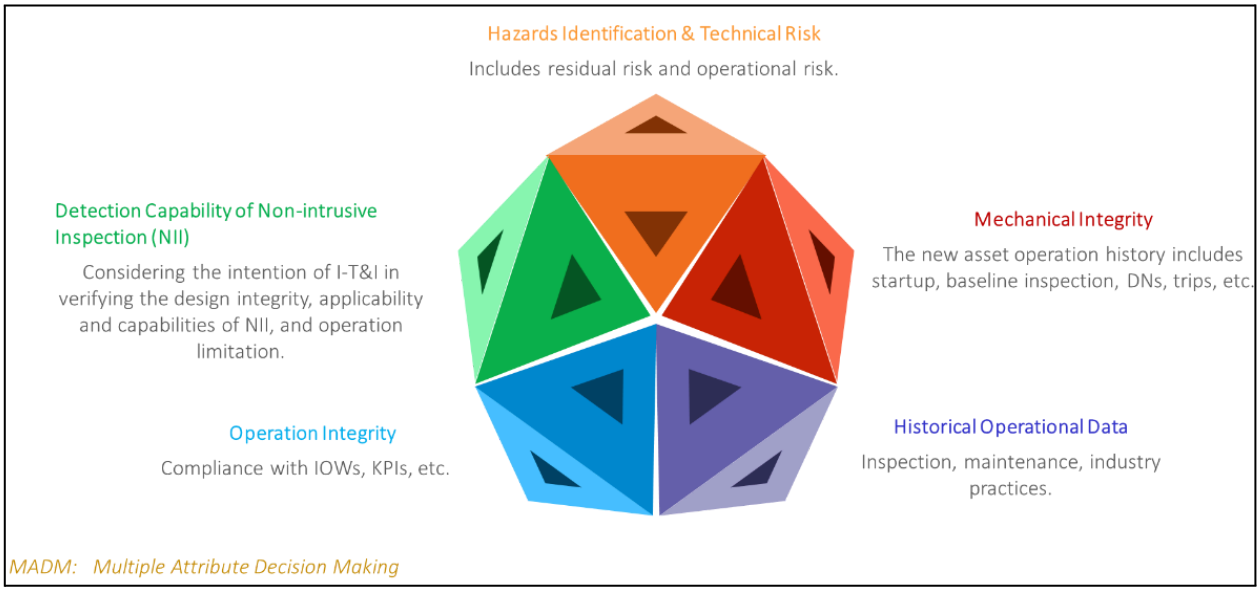

Figure 1: Dimensions of integrity evaluation

These 5 dimensions are cascaded into eleven sub-elements, as illustrated in Figure 1:

1. Evaluating the inherent risk to each piece of equipment, including the residual and operational risks.
2. Determining the potential damage mechanisms based on the material of construction, process, and operating conditions.
3. Reviewing the inspection histories of other sister plants and the industry practices and experience.
4. Reviewing the industry historical data and best practices.
5. Verifying the design integrity during the initial TA.
6. Reviewing the fabrication and construction records.
7. Reviewing the operation and maintenance history.
8. Verifying compliance with the corrosion management program, KPIs, and integrity operating windows [29, 30, 31].
9. Reviewing the operation system configuration, i.e., redundancy, isolation, etc.
10. Evaluating the applicability of NII.
11. Validating the initial TA requirements stated in the relevant regulations and legislations.

Figure 2 provides an overview of the methodology concept and basic components.

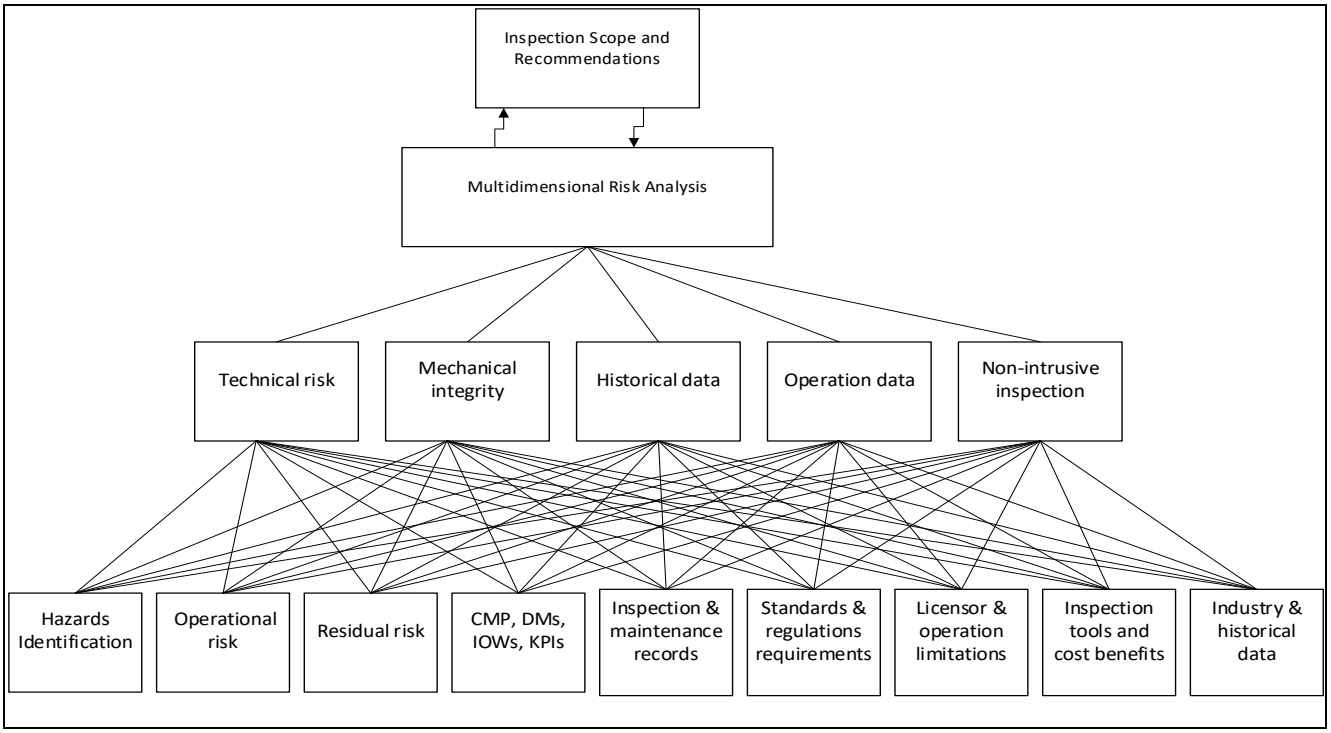

Figure 2: Overview of the methodology

III. CORROSION MANAGEMENT

Materials and corrosion reviews should address all material, corrosion, and welding issues, along with in-place corrosion monitoring and control measures. Corrosion control documents (CCD) detail design features and operating requirements related to materials selection, coatings, cathodic protection, inhibitors, chemical treatment, corrosion allowances, monitoring and inspection, post-weld heat treatment if needed, scraping, and microbiologically induced corrosion control. API RP 970 [34] provides CCD guidelines specific to refining. The effectiveness of the corrosion management program is assessed by reviewing CCDs and IOWs, including checking chemical treatment, wash water systems, and damage mechanisms. The CCD shall be utilized for the following purposes:

1. Ensure all equipment is included in the CCD with appropriate materials and corrosion control measures.
2. Review and update damage mechanisms in the corrosion loop diagrams from the detailed design phase. This requires a thorough review of design data, process information, materials, and available inspection data. Figure 3 illustrates the process of Damage Mechanism Review (DMR)

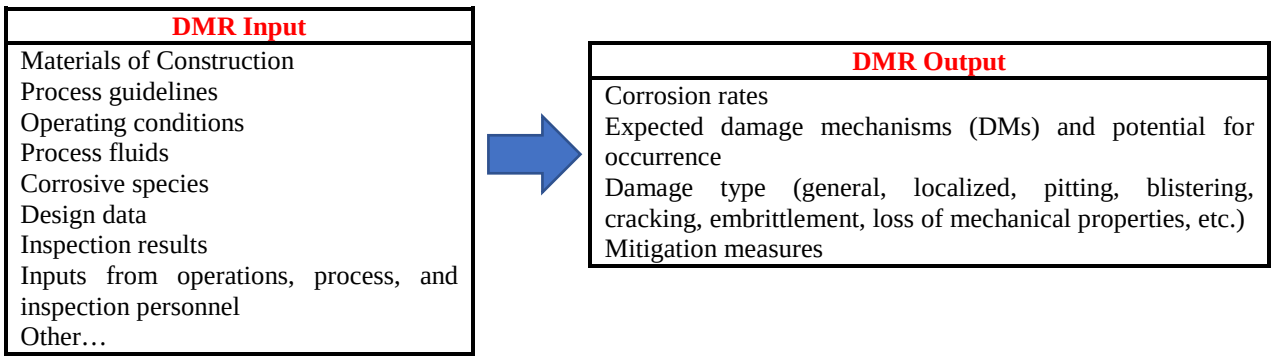

Figure 3: Overview of DMR

IOWs set limits for process variables impacting equipment integrity if operations deviate for a given time [33], the DMR involves identifying the type of damage (e.g., thinning, pitting, or cracking) expected for each asset and reviewing the established IOWs and their related details (service & operating parameters, tag, values, source, minimum, maximum, measuring unit, frequency, IOW Type, root cause of any deviation, associated risk, required action, and consequences when minimum or maximum is exceeded). Additionally, it includes a review of direct corrosion data, such as probes/coupons in correlation with the On-stream inspection (OSI) data. The following summarizes the main items that need to be checked:

- Corrosion monitoring systems, trends, performance reports, and adequacy and direct corrosion monitoring (i.e., probes/coupons). Sampling points' parameters data that are part of the Corrosion Management Solution (CMS).
- Inspection data such as OSI, corrosion monitoring locations (CMLs), i.e., numbers, locations, and inspection technique, positive material identification (PMI), injection points, and corrosion under insulation (CUI) plans.
- Completed and opened management of change (MOC) and changes in process operating parameters, IOW parameters, plant's capacities/throughput, and any plans.
- Maintenance and reliability reports, bad actor lists, failure reports, and other statistics, including replacement frequencies.
- Review risk-based inspection (RBI) assessments' recommendations.
- Risk assessment is typically applied as an aid to the decision-making process. As all possible options are evaluated, it is critical to analyze the level of risk introduced with each option. The analysis addressed the inherent criticality of equipment that has two dimensions: asset configuration and utilization. The first dimension (asset configuration) considers the availability of redundancy and buffers. As the redundancy level and buffer capacity increase, the criticality of the assets decreases. Asset configuration has four levels (1, 2, 3, and 4). Level 1 represents the most critical situation, where the asset has no redundancy and no downstream buffer. Level 2 presents the case where the asset has a downstream buffer only, while Level 3 is for the asset with redundancy only. Finally, level 4 represents the scenario where the asset has redundancy and a downstream buffer or more than one redundancy level, which is the least critical scenario. Therefore, in addition to the initial Risk-based Inspection (RBI) assessments, a qualitative approach aligned with API RP 580 was implemented to determine the inspection schema of each piece of equipment. This qualitative risk-based approach requires data inputs based on descriptive information using engineering judgment and experience as the basis for the analysis of the probability and consequence of failure.
- Verify the as-built design and materials of construction and perform comparative analysis between operating conditions and design parameters (temperature, pressure, flow, composition, etc.).
- Other items to evaluate include equipment performance, such as thermal efficiency, the output specification (e.g., columns, reactor, recovery, etc.), and licensors' technical alerts/recommendations.
- Review any deficiencies/issues found during hydrotest and lay-up in the pre-commissioning phase and/or mothballing.

3.1 In-Service Inspection Review

Operational experience is beneficial in confirming the theoretical assessments utilized in FEED and detailed design. Inspection histories of other equipment documented the types and sizes of any flaws found in service (or the absence of flaws), indicating the required inspection for other similar new equipment. This is applicable only if the conducted inspection was effective for the anticipated level of degradation and potential damage mechanisms. The area inspector and corrosion engineer to discuss with the process engineer the following key issues:

- Changes in process parameters from the original design and the adopted MOC.
- Changes in the plant layout or routing of the process fluids, addition or subtraction of the

static equipment, and the adopted MOC procedures.

- Any process upsets and their impact on the equipment integrity.
- Existing inspection issues in the plant.
- Major findings from the sister Plants/Units' previous TA and the remedial actions taken.
- The following step-by-step procedure should be applied to all static equipment on the subject plant:
- Conduct a systematic review of the inspection record for each equipment in the plant. Consider the temperature and pressure conditions, the corrosiveness of the streams, the material of construction, and the corrosion allowance.
- Evaluate the adequacy of the implemented inspection programs based on the conditions and the DMs within each corrosion loop.
- Verify the integrity and reliability of the equipment based on the available sister equipment's inspection history findings, inspection scope coverage, and potential damage mechanisms.
- Evaluate the effectiveness of the OSI program for the equipment and ensure coverage of the potential damage mechanisms. The review shall be extended to the presence of the equipment OSI drawings, location/ distribution of the CMLs, the adequacy of CMLs' types and distribution, and the OSI history results for high corrosion rate and low remaining life.
- Review inspection reports for equipment within each corrosion loop and thoroughly analyze for any observations or concerns that could result in a potential failure or increase risk in the plant.
- Evaluate the extent of the inspection and the monitoring routine/scope for all equipment. Based on the process, stream conditions, and potential damage mechanisms for the equipment, check if the existing inspection practices are adequate to completely validate and monitor the integrity of equipment and piping. If discrepancies are found, recommendations should be given for the appropriate inspection technique and the extent of the inspection. The established corrosion/erosion rate should be used (if known) for adjusting the frequency and extent of the additional inspection.
- All of the problems documented in the inspection records and reports, such as original manufacturing flaws or those related to operations. If the problems are operations-related, recommendations for follow-up inspections should be given. The active damage mechanisms in the equipment should be considered while planning the follow-up inspection recommendations.
- Review of the current operating parameters versus the design ones to identify any discrepancies that may result in a potential failure.
- Review initial and subsequent TA reports of sister assets.

3.2 Fabrication and Construction Review

One of the main objectives of performing I-TA is to inspect for fabrication and construction deficiencies that may not be revealed during the construction phase and to ensure the adequacy of the equipment design to the operating condition, i.e., design integrity. After finding all deficiencies, confirm the boundaries of each process unit and the actual mode of operation to gain a full understanding of changes in operation.

The fabrication and construction records, such as Equipment Deficiency Reports (EDRs), Non-conformance Reports (NCRs), Box up certificates, etc., shall be reviewed to verify and evaluate any residual risks or threats from the project phase. EDR is to investigate the root cause of the defective materials that have been detected after the completion of manufacturing and site arrival. Box-up is a detailed inspection of the equipment to confirm that all internal shown on design drawings have been correctly installed and inspected Typically this shall include not only trays, but also all internal parts, such as structure packing, baffles, dividers, vortex breakers, nozzles, flow distributors, piping, demister pads and catalyst supports and other mechanical parts of equipment.

whereas normal defects are mostly non-critical imperfections to the equipment's technical integrity. All corrective actions for the field observations need to be reviewed to confirm that all observations were rectified before the equipment was put into service. Finally, all Major construction observations that were rectified were tabulated in the I-TA study detailed Excel sheet and reviewed again during the study workshop stage for the final decision-making of TA categorization.

3.3 Operation and Maintenance History

One of the main criteria used to determine the process units that can be included in this study is having at least a full year of operational history. The objective of this constraint is to ensure the operation conditions reach steady states and all equipment is in operation for quite enough time to evaluate the actual operating conditions versus the design conditions. Moreover, review the maintenance history, such as the MOCs, DNs, and any other repairs or changes made to the equipment since the start-up date.

3.4 Multi-Dimensional Risk Analysis

The methodology utilizes multi-dimensional risk assessment as an aid to the decision-making process, whereas all possible TA options are evaluated, it is critical to analyze the level of risk introduced with each option. An accurate portrayal of risks is a key step in the methodology to ensure reaching the optimum inspection plan without jeopardizing asset integrity or the objective of the I-TA. The primary challenge in risk assessment lies in its multidimensional nature. A commonly accepted and relatively quantitative definition of risk is the product of probability and consequence. While this definition allows for a straightforward quantification of risk, it can sometimes be problematic, particularly when estimating probability is subjective. This is often the case with new equipment for which there is insufficient data to accurately assess the probability of failure. The methodology introduced here integrates various dimensions of risk, breaking down the probability aspect into two distinct sub-dimensions. This approach has resulted in the development of Multi-Dimensional Risk Analysis (MDRA).

The MDRA technique includes risk evaluation that is conducted for every sub-element of the MADM 5 Dimensions and their sub-elements. A 3D risk analysis, as illustrated in Figure 4, shall be conducted to evaluate three dimensions of risk:

The 1st dimension is the Confidence and Detectability. This dimension presents the SMEs' confidence in the equipment's technical integrity based on the available data and the probability of NII detecting any deterioration in the equipment's mechanical integrity.

The 2nd dimension is the severity of the operating environment and the in-place monitoring and control schema. Moreover, consider any flaw rolled over from the fabrication, installation, or construction.

The 3rd dimension is the consequences of failure. The consequence analysis shall address the inherent criticality of equipment, which has two dimensions: asset configuration and utilization. The first aspect (asset configuration) considers the availability of redundancy and buffers. As the redundancy level and buffer capacity increase, the criticality of the asset decreases. Asset configuration has four levels (1, 2, 3, and 4). Level 1 represents the most critical situation, where the asset has no redundancy and no downstream buffer. Level 2 presents the case where the asset has a downstream buffer only, while Level 3 is for the asset with redundancy only. Finally, level 4 represents the scenario where the asset has redundancy and a downstream buffer or more than one redundancy level, which is the least critical scenario.

The failure consequences can be measured in terms of their impact on people, environment, economy (i.e., production losses), and company reputation. Therefore, operating facility Health, Safety, and Environment (HSE) objectives need to be considered as part of the asset failure consequences. All assets that have been identified by risk assessment studies as safety-critical shall

be flagged, and this flag shall dominate the inspection recommendations category.

Evaluating the asset failure needs to focus on the key failure modes and damage mechanisms that lead to the worst consequences on plant availability due to their high failure frequency (e.g., chronic failures), severe failure consequences, and/or failures with extended downtime duration (e.g., maintenance difficulties, availability of repair, etc.). It is imperative to utilize actual and accurate operational data after facility start-up to establish and develop the inspection strategy. Relying on design data implies huge uncertainty and poses a great risk to the safety and availability of the facility.

Qualitatively evaluating the consequences of the failure of each piece of equipment, the primary objective of this stage is to determine what undesirable incidents could occur (the consequence) as a result of degradation that is measurable by one or more inspection techniques. The risk evaluation also includes an open-ended section to consider the in-place preventive and corrective actions to control and mitigate any potential equipment mechanical integrity deterioration.

The utilized 3D risk matrix given in Figure 4 is a volumetric cube composed of 11 volumetric layers. Each volumetric layer represents one of the 11 sub-elements.

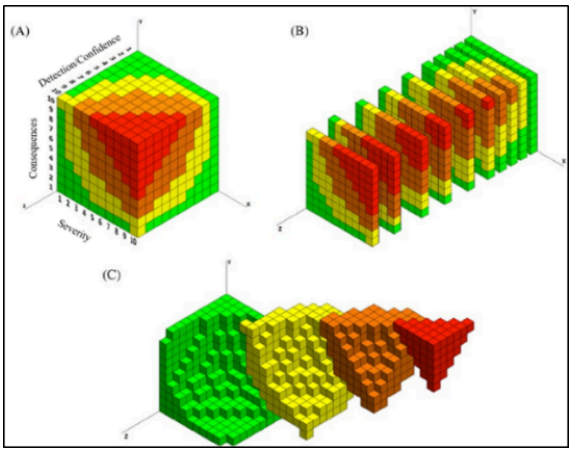

Figure 4: 3D risk matrix for the eleven volumetric layers

Risk assessment should involve the integration of information to gain insights into the operational risks associated with equipment. To achieve this, it is essential to address the following three questions:

1. What potential failures could occur?
2. What is the probability of these failures?
3. What consequences would arise from these failures?

Special course of actions should be determined for some equipment where the risk is unacceptable and cannot be mitigated to an acceptable level by NII; for these equipment items, internal inspection should be deemed necessary.

For non-pressure containing parts of equipment or parts associated with hidden failure modes Failure modes such as Fouling on shell/tube side, Leak shell to tubes, Leak tubes to shell, Tube sheet leak, Tray damage, Tray pluggage, Flooding, Down comer damage/plugging, Loss of reflux, etc. hazards should be identified and analyzed by applying failure mode and effect analysis (FMEA/FMECA). FMEA is a widely accepted methodology to determine the maintenance strategy and manage risk [27]. This methodology is basically identifying the potential failure mode of the equipment that will cause the equipment under analysis to fail to perform its intended function and estimating the consequence of that failure [28]. FMEA includes answering these questions related to failure modes (What could go wrong?) Failure causes (Why would the failure happen?)

Failure effects (What would be the consequences of each failure?). FMEA rates each potential failure mode and effect based on the following three factors:

- Severity—the consequence of the failure when it happens;
- occurrence—the probability or frequency of the failure occurring; and
- detection—the probability of the failure being detected before the impact of the effect is realized.

The risk priority is estimated by considering the severity rating, the occurrence probability rating, and the detection probability rating. Figure 5 shows an example of the FMEA for a heat exchanger tube bundle. The logic tree given in Figure 6 can be used for the risk index/priority scheme. A and B have higher priority over C when it comes to the allocation of scarce resources, and A is given higher priority than B.

#	Failure Mode	Cause(s)	Indications/ "Announcement"	Predicted Frequency	Consequences	Risk
1	Tube failure	Corrosion from fluids (shell side).	Odors at the cooling tower. Hydrocarbon detector on the tower.	Frequent—has happened twice in ten years.	Hydrocarbon is at higher pressure than the cooling water. Therefore flammable materials could enter the cooling tower and cause a major fire.	A
2	Tubesheet failure	See tube failure. Vibration of the tubes may cause the sheet to fail even if the tubes hold up.	See #1.	Rare	See #1.	B

Figure 5: FMEA for heat exchanger tube bundle

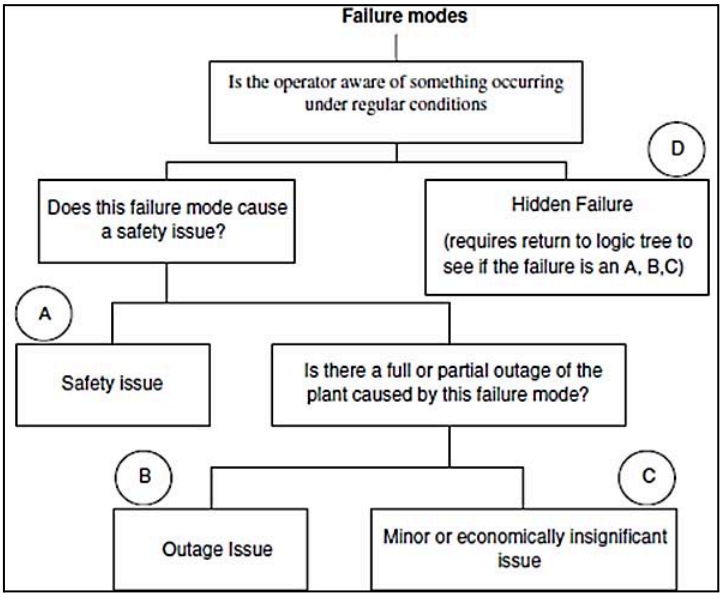

Figure 6: Logic tree analysis

IV. DELPHI WORKSHOP

The challenges in asset management (AM) in the current industrial era generally include organizational challenges that entail the integration of all stakeholders across the organization hierarchy for the successful implementation and improvement of AM practice [15]. The main characteristic of MADM problems is that there are usually a limited number of predetermined alternatives that are associated with a level of achieving the attributes. Based on the attributes, the final decision is to be made [6].

Therefore, an in-person workshop shall be conducted and should start with a process presentation of the section of the plant that is covered in the study, and should highlight all commissioning and startup challenges, process and operation concerns, and history. Other disciplines will follow in presenting their findings and recommendations. A Master Sheet shall be used to perform a thorough review of every piece of equipment and shall be used to document all discussion items, any further action, conclusions, and recommendations.

The Delphi technique effectively reaches consensus and forecasts future events by collecting opinions from subject matter experts (SMEs). The Delphi method involves structured communication, anonymity, controlled feedback, iteration, and formal group judgment.
The list of required documents, records, and data outlined in the next section (Case Study) should be reviewed and utilized during the workshop to reach a consensus among the Study team. The decision-making process includes the following steps:

- Identifying a wide range of potential options, including novel approaches.
- Effectively evaluate the relative merits of each inspection option.
- Allowing for appropriate levels of input, review, and analysis.
- Assessing all applicable options and the challenges associated with each.
- Employing timely and fair decision-making methods to reach a consensus.

The study recommendations shall be categorized as follows:

- Category I: Equipment that needs to be taken out of service for a full internal inspection. This also includes equipment that was selected to be a sample (Category III) for other equipment, e.g., fin-fan coolers, heat exchangers, drums, etc.
- Category II: Equipment for which NII can be performed in lieu of internal inspection.
- Category III: Equipment that is part of the sampling equipment group. For example, if there are six similar fin-fan coolers, then two coolers will be laid under Category I, and the remaining four coolers will be laid under Category III.
- Category IV: Equipment that needs internal inspection, but the scope is optimized. For example, the inspection of the shell and tube heat exchanger can be performed without pulling out the tube bundle.

V. DECISION-MAKING GUIDANCE

This section offers a decision-making process to determine the appropriateness of considering NII for inspecting a specific piece of equipment.

- Identify the equipment for which NII should not be considered or where the required information cannot be obtained from such an inspection.
- Confirm that the equipment is intrinsically suited to inspection by non-intrusive means; that is, there are no immediately obvious impediments to NII being undertaken. These include factors such as where there is no access to the equipment exterior, extreme surface temperatures, geometry constraints, and restrictions to access, as well as any requirement for the inspection of internal fittings.
- Identify equipment with no previous in-service inspection history or for which there is a reason that the inspection history may no longer be relevant (due, for example, to a change in process conditions) should not normally be considered for NII.
- Identify if there is other equipment for which the inspection history may be directly relevant to the equipment under consideration. Substantially the same in terms of design, geometry, construction, and conditions of service (i.e., normally empty /full, etc.), and there are no factors with potential to cause a difference in nature, distribution, or rate of degradation that can be identified.
- Identify opportunities for internal inspection; when the equipment is to be opened for other reasons, advantage should be taken of the opportunity to perform an internal visual inspection. This does not mean that NII should not be done. However, if it is intended to do NII in parallel with internal inspection,

then this can be done without additional justification.

- Identify the effectiveness and confidence of NII to determine whether NII is appropriate in principle. This requires consideration of how confidently potential flaw types and locations can be predicted, the effectiveness of previous inspections, and the severity and rate of any known or predicted degradation. The decision on whether NII is appropriate in principle is based, to a large extent, on confidence in being able to predict all active degradation mechanisms and, hence, specify methods capable of identifying the associated flaws. The ability to predict degradation mechanisms depends on several factors such as uncertainty in the equipment condition due to confidence in the quality control processes during fabrication, installation, and construction, consequences of failure, severity, detectability, in-place IOWs, process control and monitoring, etc.

VI. CASE STUDY

The proposed methodology was applied to several newly constructed refineries and gas plants that had completed at least one year in stable operation. One of these use cases was for a clean fuel expansion project that consists of Naphtha Hydrotreating (NHT), Continuous Catalytic Regeneration (CCR), Reforming and Isomerization Units to upgrade the diesel and gasoline produced by a refinery, hence, to improve refinery profitability. This is done by decreasing the sulfur content in gasoline to 10 ppm_w S, benzene content to less than 1% vol, and aromatics content to less than 35% vol.. CFP also produces ultra-low sulfur diesel to 10 ppm_w and low sulfur diesel to 500 ppm_w with T85% distillation at 350°C. NHT capacity of 138,000 BPSD, which is further split into two streams after treatment into Light naphtha and Heavy naphtha. The heavy naphtha is further processed in Reforming CCR with a capacity of 90,000 BPSD, whereas the Light naphtha with the other light naphtha available in the refinery, is processed in the Isomerization unit with a capacity of 64500 BSD.

The most crucial phase of the Study is data collection, reconciliation, and quality checks for accuracy:

General

- Manufacturers' recommendations for proprietary equipment.
- Equipment technical information, such as data sheet, design drawings, and as-built drawings.
- Complete list of past failures associated with materials, welding, or corrosion.
- Complete list of challenges and changes encountered during commissioning, startup, and the one year of continuous operation.
- Failure analysis reports and RCA.
- TA reports from sister plants/units.
- Incident investigation reports.
- Historical capacity/process changes.
- Safety Management System (SMS) compliance reports.
- List of all MOCs, either closed or opened.

Process Engineering

- Operation manual and process description.
- Design feed characteristics, product specifications, and properties, and controls.
- Material and Heat Balances of the plant.
- Battery limit conditions.
- Process upset history and IOWs trends from the start-up for at least one year.
- Equipment performance evaluation spreadsheets, software, and simulation models.
- Operations: operation modes and parameters, trending procedures, HAZOP studies.
- Instrumentation and control systems: ESD and control valves' specifications, performance, and maintenance practices.
- Tendency to fouling, carry over, or other operation challenges.

Inspection

- Final Quality Dossier (FQD) to verify and evaluate any residual risks or threats from the project phase. All NCRs were reviewed during the study to ensure that all NCRs were closed with proper corrective action.

- History of equipment preservation.
- Box-up inspection reports.
- box-up inspection report.
- Equipment inspection history and piping replacement.
- Documentation for all inspection programs, dead legs, small bore piping/nipples, vents, drains, and corrosion under insulation.
- Inspection: OSI and CMLs: isometric drawings and results.
- Outstanding and completed Defect Notifications (DNs).

Materials, Welding & Corrosion

- Corrosion management techniques and control methods.
- Leakage history.
- Listing of IOWs with targets, for NHT/CCR, the IOWs consist mainly of parameters associated with the NHT reactor feed heater's skin temperatures, Reaction feed/effluent exchangers, stripper feed/reactor effluent exchanger, Reactor effluent air condenser, separator drum, Reactor effluent air condenser, Regenerator, stripper reflux drum, and catalyst lift velocity. For the Isomerization unit, the IOWs consist mainly of parameters such as Caustic concentration, water pH, Chloride content, etc., associated with Naphtha feeds surge drum, Mercury guard bed, Sulfur guard bed feed/effluent exchangers Naphtha feeds steam heater, Naphtha feeds sulfur guard bed, and Naphtha feeds sulfur guard bed.
- Corrosion, cracking, and fouling problems.
- Cathodic protection systems conditions.
- Corrosion loops, annotated with damage mechanisms.

Heat Transfer Equipment

- Original thermal calculation.
- Original mechanical calculation.
- Repair history for all heat exchanger equipment.
- Mechanical drawings for all heat exchangers equipment.
- Heater original thermal calculation.
- Heater original mechanical calculation.
- Heater operation and repair history.
- Heater inspection history, including the UT tube thickness readings.
- Process parameters trend.
- Operation vs. design condition for all heat exchangers.
- Heater process parameter trends include tube skin temperature, such as heater duty trend, process flow rate trend, inlet & outlet temperatures trend, fire box Temperature trend, stack temperature trend, heater draft trend, heater excess O_2 trend, fuel rate trend, fuel temperature trend, and tube skin temperature trend.
- Baseline UT Measurements for the radiant tubes section of all fired heaters.

VII. RESULTS

In the final stage of the risk analysis, the scheme of examination is established for every piece of equipment. It is important to note the interaction between the above stages. The scheme of examination and scope of work were determined based on the type and location of possible deterioration, the inherent operational and technical risk, and the optimum essential inspection effectiveness category to achieve the required risk reduction. Eventually, the inspection and testing techniques, along with the coverage percentage, were selected based on the Inspection Effectiveness Tables. Figure 7 shows the distribution of the recommendations, where 62.21% of equipment falls under Category I, which requires full internal inspection, and 3.97% of equipment falls under Category IV, which requires internal inspection but with an optimized scope.

In total, internal inspection is required for 66.18%. On the other hand, NII is found to be an equivalent substitute to internal inspection for 25.05% that falls under Cat. II. The scope of work for the remaining 8.77% falls under Category III and will depend on the inspection results of other identical equipment (i.e., no inspection would be required if the inspection was performed on other identical equipment with no major findings.

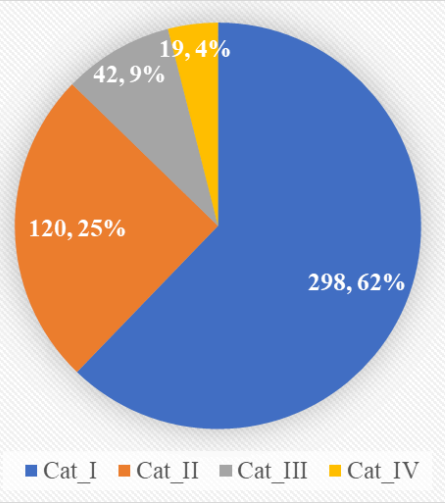

Figure 7: Distribution of the study recommendations

All use cases resulted in around a 40-50% reduction in the original scope. In other words, we optimized the inspection and maintenance resources by focusing on the necessary scope. This reduction in the TA scope means a shorter duration of the TA, which in turn increases plant availability and minimizes business interruption costs. Having a controlled TA scope means less complexity, which translates to a minimum risk of cost overrun and schedule slip. Minimizing personnel safety risk is achieved by avoiding unnecessary maintenance and inspection activities, such as confined space work. Avoiding unnecessary internal inspection and exposing the equipment to the atmosphere can minimize disposal, water washing, steam out, and chemical usage such as alkaline and acidic solutions, i.e., Green TA!

VII. CONCLUSION

There are several MADM methodologies, such as AHP; however, none of these methodologies explicitly address or quantify the risk. This paper introduced a novel hybrid methodology that combined the MADM technique with MDRA to determine the initial TA inspection scope. The methodology presented here was developed at both the strategic level of optimizing the scope of TA toward establishing a cost-effective organization and the tactical level, where a detailed framework was presented to conduct a successful optimization study.

This new methodology forms a corpus of principles, routines, and processes that were deployed at different plants and found to be a sound basis for managing the development of the initial TA inspection scope. The paper presented a use case at a new refinery to identify the appropriate and adequate initial TA inspection scope to aid in optimizing the TA scope, delivering production operational targets, and avoiding unnecessary replacement of internal parts (e.g., catalysts, desiccants, etc.) due to exposing the equipment to internal inspection. The study resulted in around a 50% reduction in the original scope, which minimized the TA duration, increased plant availability, and minimized business interruption costs and environmental impact. Thus, promoting a more sustainable 'Green TA' approach that reduces both business disruption and environmental footprint.

For future work, this innovative methodology should be expanded across diverse plant types, incorporating real-time data analytics or machine learning into the risk assessment, and expanding the framework to cover post-TAs.

REFERENCES

1. Lenahan, Tom, and Tom Lenahan. Turnaround, Shutdown and Outage Management: Effective Planning and Step-by-Step Execution of Planned Maintenance Operations.. Oxford ; Elsevier/ Butterworth-Heinemann, 2006. Print.

2. Huairui Guo et al. “On Determining Optimal Inspection Interval for Minimizing Maintenance Cost.” 2015 61ST annual reliability and maintainability symposium (RAMS 2015). vol.. 2015-. NEW YORK: IEEE, 2015. 1–7. Web.
3. Leoni, Leonardo et al. “On Risk-Based Maintenance: A Comprehensive Review of Three Approaches to Track the Impact of Consequence Modelling for Predicting Maintenance Actions.” Journal of loss prevention in the process industries 72 (2021): 104555-. Web.
4. Murthy, A.S.R. and Naikan, V.N.A. (1996), “Condition monitoring strategy: a risk-based interval selection”, Int. J. Prod. Res., Vol. 34 No. 1, pp. 285-96.
5. Hey, R.B. (2019), Turnaround Management for the Oil, Gas, and Process Industries: A Project Management Approach, Gulf Professional Publishing.
6. Ekel, P., Pedrycz, W. and Pereira, J. (2019), Multicriteria Decision-Making under Conditions of Uncertainty: A Fuzzy Set Perspective, Wiley.
7. Bertolini, M et al. “Development of Risk-Based Inspection and Maintenance Procedures for an Oil Refinery.” Journal of loss prevention in the process industries 22.2 (2009): 244–253. Web.
8. Alfares, Hesham K. Applied Optimization in the Petroleum Industry. Cham: Springer, 2023. Web.
9. Arunraj, N. and Maiti, J. (2007), “Risk-based maintenance – techniques and applications”, Journal of Hazardous Materials, Vol. 142 No. 3, pp. 653-661.
10. Khan, K., Sadiq, R., & Haddara, M. (2004). Risk-based inspection and maintenance (RBIM): multi-attribute decision making with aggregative risk analysis. Process Safety and Environmental Protection, 82, 398–411.
11. American Society of Mechanical Engineers Code Committee SC6000. (2000). Hazardous release protection. New York, NY: ASME.
12. Krishnasamy, L., Khan, F., & Haddara, M. (2005). Development of a risk-based maintenance (RBM) strategy for a power-generating plant. Journal of Loss Prevention in the Process Industries, 18, 69–81.
13. Kumar, U. (1998). Maintenance strategies for mechanized and automated mining systems: a reliability and risk analysis based approach. Journal of Mines, Metals and Fuels, 46(11–12), 343–347.
14. Van Heel, K. A. L., Knegtering, B., & Brombacher, A. C. (1999). Safety lifecycle management. A flowchart presentation of the IEC 61508 overall safety lifecycle model. Quality and Reliability Engineering International, 15, 493–500.
15. S. More, R. Tuladhar, D. Grainger, and W. Milne, “Maintenance decision-making and its relevance in engineering asset management,” Maintenance, Reliability and Condition Monitoring, Vol. 4, No. 1, pp. 1–17, Mar. 2024, https://doi.org/10.21595/marc.2024.23687
16. Saaty, T.L. (1980), The Analytic Hierarchy Process, McGraw–Hill, New York.
17. Golden, B.L., Wasil, E.A. & Harker, P.T. (1989), The Analitic Hierarchy Process, Heidelberg.
18. Wang, Y., Cheng, G., Hu, H., Wu, W., 2012. Development of a risk-based maintenance strategy using FMEA for a continuous catalytic reforming plant. J. Loss Prev. Process. Ind. 25 (6), 958–965.
19. Alsyouf, I., 2007. The role of maintenance in improving companies’ productivity and profitability. Int. J. Prod. Econ. 105 (1), 70–78.
20. William Fauriat, Enrico Zio, Optimization of an aperiodic sequential inspection and condition-based maintenance policy driven by value of information, Reliability Engineering & System Safety, Volume 204, 2020, 107133, ISSN 0951-8320, https://doi.org/10.1016/j.ress.2020.107133.
21. Barlow RE, Proschan F. Mathematical theory of reliability. 17. Siam; 1967.
22. Abdel-Hameed M. A gamma wear process. IEEE Trans Reliab 1975;24(2):152–3.
23. Othman MR, Idris R, Hassim MH, Ibrahim WHW (2016) Prioritizing HAZOP analysis using analytic hierarchy process (AHP). Clean Technol Environ Policy. https://doi.org/10.1007/s10098-016-1104-4

24. J. M. Lafleur, "Probabilistic AHP and TOPSIS for multi-attribute decision-making under uncertainty," 2011 Aerospace Conference, Big Sky, MT, USA, 2011, pp. 1-18, https://doi: 10.1109/AERO.2011.5747655.
25. Optimising Shutdown Strategies (oilandgasiq.com) https://www.oilandgasiq.com/oil-and-gas-production-and-operations/whitepapers/optimising-shutdown-strategies.
26. Duffuaa, Salih O, A Raouf, and A Raouf. Planning and Control of Maintenance Systems: Modelling and Analysis. Second edition. Cham: Springer Nature, 2015. Web.
27. Khanfri, N. E.H et al. "New Hybrid MCDM Approach for an Optimal Selection of Maintenance Strategies: Results of a Case Study." SPE production & operations 38.4 (2023): 724–745. Web.
28. Meyer, N., Cho, J. J., and Phillips, R. G. 2014. Mitigating HS&E Risks for Oil & Gas Services Using a Comprehensive Risk Management Program during New Product Development. Paper presented at the SPE Middle East Health, Safety, Environment & Sustainable Development Conference and Exhibition, Doha, Qatar, 22–24 September. SPE-170440-MS. https://doi.org/10.2118/170440-MS.
29. Lagad, Vishal, and Vibha Zaman. "Utilizing Integrity Operating Windows (IOWs) for Enhanced Plant Reliability & Safety." Journal of loss prevention in the process industries 35 (2015): 352–356. Web.
30. Arena, Edoardo et al. "RBI-IOWs Integrated Approach to Risk Assessment: Methodological Framework and Application." Journal of loss prevention in the process industries 79 (2022): 104838-. Web.
31. Wilson, Peter T. "Managing the Mechanical Integrity of Pressure Equipment Using a Layers of Protection Framework and Incorporating Integrity Operating Windows." Journal of loss prevention in the process industries 79 (2022): 104821-. Web.
32. https://www.netzerotc.com/wp-content/uploads/2023/02/ogtc-and-abb-non-intrusive-inspection-survey.pdf
33. API, 2021. Recommended Practice 584, Integrity Operating Windows, 1st edition. American Petroleum Institute, Washington, D.C.
34. API, 2023. Recommended Practice 970, Corrosion Control Document Systems, 2nd edition. American Petroleum Institute, Washington, D.C.

This page is intentionally left blank

Search of Floating Mines by Unmanned Aerial Vehicles using Kinematic Projection Methods

Ivan Aftanaziv

Lviv Polytechnic National University

ABSTRACT

The question of demining sea raids and ports, which is relevant for Europe in the period of active deployment of military confrontations on its territory, is considered. It is proposed to combine the search capabilities of unmanned aerial vehicles (UAV) with the ability of trawler boats to clear floating mines. The optimal trajectory of search movements of UAV along the Archimedean spiral is proposed. An appropriate number of UAV that can effectively search for floating mines simultaneously is determined.

Mine detonation with warheads dropped from an aerial liquidator drone is proposed as one of the most effective ways of the disposal of mines.

The proposed method can be used to manage the search movements of UAV, to process the data provided by them about the detected floating mine, and to clarify the coordinates of the floating mine. A corresponding block diagram for computer software is proposed.

Keywords: floating mine, demining, trawler boat, aerial vehicle, unmanned aerial vehicle, drone, coordinates, search.

Classification: DCC Code: 623.45

Language: English

Great Britain Journals Press

LJP Copyright ID: 392923
Print ISSN: 2631-8474
Online ISSN: 2631-8482

London Journal of Engineering Research

Volume 25 | Issue 2 | Compilation 1.0

Search of Floating Mines by Unmanned Aerial Vehicles using Kinematic Projection Methods

Ivan Aftanaziv

ABSTRACT

The question of demining sea raids and ports, which is relevant for Europe in the period of active deployment of military confrontations on its territory, is considered. It is proposed to combine the search capabilities of unmanned aerial vehicles (UAV) with the ability of trawler boats to clear floating mines. The optimal trajectory of search movements of UAV along the Archimedean spiral is proposed. An appropriate number of UAV that can effectively search for floating mines simultaneously is determined.

Mine detonation with warheads dropped from an aerial liquidator drone is proposed as one of the most effective ways of the disposal of mines.

The proposed method can be used to manage the search movements of UAV, to process the data provided by them about the detected floating mine, and to clarify the coordinates of the floating mine. A corresponding block diagram for computer software is proposed.

It has been established that using the proposed search method and at the speed of UAV 5-5.5 m/s, it is possible to survey up to 6 square kilometers of sea every hour. At the same time, it is possible to save up to 20 liters of fuel for the trawler boat.

Keywords: floating mine, demining, trawler boat, aerial vehicle, unmanned aerial vehicle, drone, coordinates, search.

Author: Lviv Polytechnic National University, Lviv, Ukraine.

ABSTRAKT

Przez nie danych na temat wykrytej pływającej miny oraz do ustalania współrzędnych pływającej miny. Zaproponowano odpowiedni schemat blokowy oprogramowania komputerowego.

Ustalono, że przy zastosowaniu proponowanej metody poszukiwań i przy prędkości BSP 5-5,5 m/s możliwe jest przeszukanie do 6 kilometrów kwadratowych morza w ciągu godziny. Jednocześnie możliwe jest zaoszczędzenie do 20 litrów paliwa dla trawlera.

Słowa kluczowe: mina pływająca, rozminowywanie, trawler, statek powietrzny, bezzałogowy statek powietrzny, dron, współrzędne, poszukiwanie.

I. INTRODUCTION

It should be noted that during the last decades, due to the use of state-of-the-art computer technologies at the stage of design and calculations, huge progress has been made in the improvement of military equipment. Besides, the main trend in almost all areas of building military equipment and weapons is minimization of human participation in setting up and using weapons.

This feature is also characteristic of the navies of the developed countries of the world, particularly in the field of mining and demining sea routes and water areas of ports. The latest materials and explosives, modern capabilities of perception, processing, and response to electromagnetic, acoustic, and noise disturbances of the sea surface by ships or submarines turn mining into a formidable weapon of active response. Thus, modern bottom mines can float to the surface (model MN103-bottom non-contact mine) or

torpedo enemy ships at the right time by remote command (model Mark 60 Captor).

Of course, with the improvement of mine weapons, the technical means of demining both individual mines and minefields are improved. Here, special attention is paid to the safety of people clearing mines. Remote control of robotic demining equipment is recognized as the most effective method of personnel protection. Therefore, remote-controlled unmanned underwater demining devices (project for the US Navy Proteus) were developed and put into practical use. Also widely used are the so-called "kemikaze" torpedo-robots, which, upon detecting a depth- or a bottom mine, approach it and explode. Due to detonation or mechanical damage, the explosion of a "kemikaze" torpedo-robot provokes the explosion of a depth mine. Thus, the danger of detonation of ships or other floating means by this mine is neutralized.

Certainly, special trawler boats are still widely used for demining and etching the surface of the sea. The history of using trawler boats for neutralizing floating and anchor mines goes back almost a century. The beginning of their use practically coincides with the period of the beginning of active mining of seas. However, nowadays even such an ancient method of demining is being modernized and improved. These improvements consist in equipping the minesweepers with unmanned floating and aerial vehicles for searching for mines and remotely controlled charges for detonating them.

At the same time, other search methods are being improved. A vivid example of successful use of unmanned aerial vehicles (UAV) for mine searching is the method of searching by magnetometric sensors attached to these devices developed by the Ukrainian State Research Institute for Testing and Certification of Weapons and Military Equipment. An aircraft with magnetometric transducers suspended on cables at a height of 10-15 meters above the ground flies along a given trajectory. The signal from the sensor about the detected mine is transmitted to the command post, where it is processed in order to determine the exact coordinates of the detected mine. The ensured accuracy of determining the coordinates of 82- and 120-millimeter mines here reaches a discrepancy of only a few centimeters [1]. This method of searching for mines by magnetometric sensors suspended from a UAV could be successfully used to search for mines floating on the water surface. However, such studies have not yet been conducted.

It should be noted that in contrast to anchor and bottom mines, the installation of which is necessarily accompanied by the fixation of anchorage locations on the corresponding mining maps of a marine water area, the placement of floating mines is not fixed and is constantly changed by winds and currents, as well as wave disturbance of the sea surface. Moreover, even a floating mine detected but not neutralized in time remains dangerous, since it is not fixed at the place of detection and continues to move in the water.

Floating mines pose a certain danger not only to ships, but also to the civilian population on sea coasts. Driven by the waves to the shallows of the coastline, these mines can explode even from shock contact with the seabed of the coastal shoal. And their explosions on coastal shoals threaten the lives and health of people working or resting on the coast. Such an unfortunate event that took the life of one person and severely injured another happened on the seashore near the city of Odesa (Ukraine) in June 2022. A mine that was torn from the anchor, which was installed by the Russian military to block the ports of Odesa, was torn from the anchor and washed by the waves to the shore of the sea beach. And it was her explosion that caused the death and serious injuries of people. A similar situation, accompanied by the death of a person, was repeated here in July of the same year.

Also, floating mines not only create obstacles and danger to shipping, but also threaten people's lives and health. And according to the press service of the Ukrainian Navy, in the first four months of the Russian aggression, about 400 mines of various types were placed in the waters of the Black Sea by the troops of the Russian Federation.

The importance of the ability to ensure the stability of sea and river ports was clearly illustrated by the military events of 2022 on the territory of Ukraine. Ukraine's ports in the Black Sea, mined by the troops of the Russian aggressor, have blocked Ukraine's ability to supply grain crops to world markets. Due to the fact that Ukraine was and remains the main supplier of grain to the markets of African countries, the long-term blockade of Ukrainian seaports led to a rapid increase in the cost of grain on world markets. Moreover, there is a very real threat of famine in economically backward African countries, for which Ukraine is the main supplier. It is natural that this will provoke social unrest due to the danger of possible starvation of the population.

This situation once again emphasizes the importance of ensuring the stability of seaports, and accordingly, the related problem of quick and guaranteed effective demining of sea ship raids and port water areas.

Therefore, the problem of improving the methods of searching for and neutralizing sea mines of all types and varieties, including floating mines, remains relevant.

II. REVIEW OF PREVIOUS STUDIES

Despite the appearance of quite original methods and equipment for finding mines and demining, the method of demining minefields with self-propelled trawls is still the most widely used. Mostly these are specially equipped boats like the Swedish SAM-3 or the American SAM-05, which are adapted to the perception and resistance to mine explosions [1]. Quite often, current trawler boats are equipped with various simulators of vibrations, noises and magnetic field disruptors to simulate ships moving on raids and provocations of mine detectors to explode. Current trawler boats are mainly collapsible pontoon boats with a speed of 6-8 knots, which are easily transported by airplanes to the required areas of the sea.

So-called helicopter trawls can be considered a certain alternative to self-propelled trawls [2]. These trawls are also equipped with magnetic field generators and cutting equipment for neutralizing anchor mines. A typical representative of such trawls is the Harris MK-105 hydrofoil trawl.

When it comes to demining large areas of sea water area, then, of course, preference is given to large-tonnage specialized trawlers. In fact, it is a large universal platform for basing, transporting surface, air and unmanned mechanisms for detecting all types of mines without exception and their neutralization. The displacement of such a trawler ship reaches 3,500 tons, the speed is 15-20 knots. In the process of demining, such a ship explores and clears 10-20 square kilometers per hour and up to 500 square kilometers per day.

The improvement of modern means of heliolocations and radar and other search equipment contributed to the fact that aerial vehicles are increasingly used to search for mines. For example, paper [1] provides information on the creation of special magnetometric transmitters in Ukraine, which are suspended from UAV on cables to search for unexploded explosive mines and objects. However, data on the possibility of using magnetometric sensors to search for floating mines are not given in this paper.

Sometimes a system of connected pontoons, on which generators of magnetic, acoustic and electromagnetic fields are installed, is used to simulate the noises and fields of the ship. An aircraft, such as a helicopter or a powerful drone, transports these pontoons on the surface of the sea, imitating a ship and provoking a mine explosion [1]. Such pontoon systems are manufactured by Thales Australia.

To search for floating mines in areas of the sea close to the shore, helicopters or aerial drones with laser systems for scanning near-surface waters are quite often used [1]. An example of the use of such a mine detection scheme is the US Navy's base for laser scanning of the Northrop Grumman MQ-8 Fire Scout model.

A relatively new step in the research of methods of searching for floating mines is the application of unmanned aerial vehicles to search operations. In general, UAV were actually created for

reconnaissance and search operations. However, for the search for sea mines, the authors propose their use for the first time.

UAV have particularly convincingly demonstrated their effectiveness as sabotage and reconnaissance weapons on the battlefields of the Russian-Ukrainian war in 2022. Virtually silent and invisible to enemy radars, these aircraft have become indispensable for gathering useful intelligence information about the deployment of enemy equipment and personnel [3]. Equipped with modern high-resolution video equipment, these flying scouts have become an integral part of almost every military unit, even a small one [4].

And the equipping of the so-called "aerial drones" with more powerful engines and devices for transporting, holding and remotely controlled dropping of explosive charges turned them into formidable modern weapons [5]. Actually, it is the ability not only to detect small-sized objects on the ground and water surface, but also to bombard and detonate them remotely with warheads, which became the root cause of our recommendation for the use of UAV for the search and disposal of floating mines.

It should be noted that the authors of the article have some positive experience in using UAV to search for moving objects by means of kinematic projection. In particular, our scientific studies describe the schemes of using UAV in agriculture and forestry [6, 7], in cinematography [8] and aerial photogeodesy [9], in military affairs to detect the coordinates of enemy sabotage and reconnaissance UAV [10, 11, 12]. The vast majority of these studies are based on an organic combination of the reconnaissance capabilities of modern small-sized video equipment, with which UAV and drones are equipped, with the ability of highly accurate calculations of the coordinates of the spatial movements of objects using computer technology based on kinematic projection data.

These studies were based on the experience of employees of Lviv Polytechnic National University (Ukraine) in the field of aerial photogeodesy in the use of UAV to determine the coordinates of an area when compiling topographic maps [13, 14].

The kinematic projection method used by us allows determining the instantaneous coordinates and the trajectories of moving objects. Note that all the means and components of projection are moving, namely the objects of projection, "observers" and the coordinate plane with projecting rays. At the same time, all these projection objects or part of them can be in accelerated or uniform motion, and the movement of each projection component does not depend on the movement of other components [8, 10, 15].

Practical application of the theoretical foundations of kinematic projection opens new possibilities in the display of moving objects in space, in determining instantaneous coordinates of their location, and, if necessary, in determining the characteristics and components of movement [10, 11, 15].

The main goal of this study was to develop a method of searching for floating mines for demining sea and river water areas.

To achieve this goal, the following tasks were formulated:

- To develop a methodology for determining the spatial coordinates of a solid body located on the water surface by means of kinematic projection;
- To determine the optimal number of UAV for determining the coordinates of a floating mine;
- Research and development of the optimal trajectory of spatial movements of UAV when they search for floating mines;
- Creation of a software algorithm for the development of a UAV data reconciliation program when they determine the location of a floating mine.

III. PRESENTATION OF THE MAIN MATERIAL

The conducted analysis of the use of various means of searching for and neutralizing floating mines convincingly leads us to the opinion and belief that the most optimal will be an organic combination of the advantages of the use of sea floating means and flying equipment [2, 5]. In the

case of floating mines, it should be a combination of the simultaneous use of trawler boats with unmanned aerial vehicles (UAV). On a trawler boat, for example, the ARCIS Atlas Electronik model, a command post with means of controlling the search movements of aircraft and software for calculating the coordinates of detected mines, a radar station (Radar) for tracking UAV, a platform for launching and landing aircraft and, of course, should be equipped equipment for remote disposal of detected mines [1, 3].

As search aircraft, it is appropriate to use medium-sized drones or quadcopters capable of carrying portable radar equipment weighing up to 40 kg with an effective range of 200-250 m and high-resolution visualization and sea surface monitoring equipment with a range of at least 100 m [9, 13]. In the event of the need to detonate detected mines, these aircraft must be equipped with remotely controlled warhead holders. Quite a lot of types of drones meet these requirements, for example, models Predator-B (General Atomic Aeronautical Systems Inc, USA), Grand Duck (Dasso, France), etc. But the most effective, in our opinion, would be the use of a small-sized exterminator drone model Switchblade 600 for the elimination of detected mines. Its advantage, in addition to small weight and size, is the presence of GPS navigation and the ability to search for and recognize predetermined objects. The ability of this kemikaze drone to fly continuously for 30 minutes at a cruising speed of 112 km/h is also significant.

If the search for floating mines is carried out in the coastal water area of the sea, which is several kilometers away from the coast, then the command post for controlling the search work of drones is set up mainly on the shore. If the search maneuvers are carried out in the open sea in areas that are tens of kilometers away from the coastline, it is advisable to use a properly equipped trawler boat for basing, launching, guiding the work and trajectories of drone movements. Given that floating mines can move on the surface of the sea under the influence of winds, sea surface disturbances, currents and eddies, the coordinates of the location of these mines detected by drones are not constant and can constantly change. Therefore, it is advisable to constantly monitor the floating mines detected by drones, and even better, to ensure the safety of sea vessels and people, that is to destroy the mines. For this, the same search drones that are equipped with suspended ammunition instead of search equipment [4, 10] can be used.

Of course, searching for floating mines using UAV requires, in addition to appropriate weather conditions, such as wind power, certain calculated trajectories of their spatial movements. Moreover, the floating mines discovered during the previous search days will definitely change their location under the influence of winds and currents and will have to be searched for again. Therefore, when organizing search operations for the demining of certain water areas of the sea, it is appropriate to organize search operations in such a way as to cover the areas of search as widely as possible, as well as to ensure the neutralization of discovered warheads. Therefore, along with the power of search equipment, the trajectories of its movement are of great importance. At the same time, the number of simultaneously used search devices may increase, so their search modes and trajectories should be coordinated properly.

In a certain way, the search for "floating" mines is largely similar to the movement of fishing vessels when they search for shoals of fish.

The demining of sea waters from floating mines using UAV is carried out in the following sequence. The trawler 1 with four UAV of the "drone" type loaded on it, equipped with the above-mentioned search equipment, as well as explosive charges for detonating detected mines, enters the central part of the sea area allocated to it for search. Here it anchors, if the depth of the sea allows, or slowly drifts, occasionally adjusting its location near the center of the search area. Three drones with 2 radar search equipment and surveillance video cameras are launched alternately into the sky. At the first stage, the command post for controlling search operations, using the appropriate computer programs for managing search movements, arranges three drones in one line at a distance, for example, a from each other and from the command post on

the trawler. The distance a between the drones 2 is set equal to diameter d of the effective hemisphere of their search radar equipment, i.e. a=d=2r, where r is the effective search radius of the drone 2 (Fig. 1).

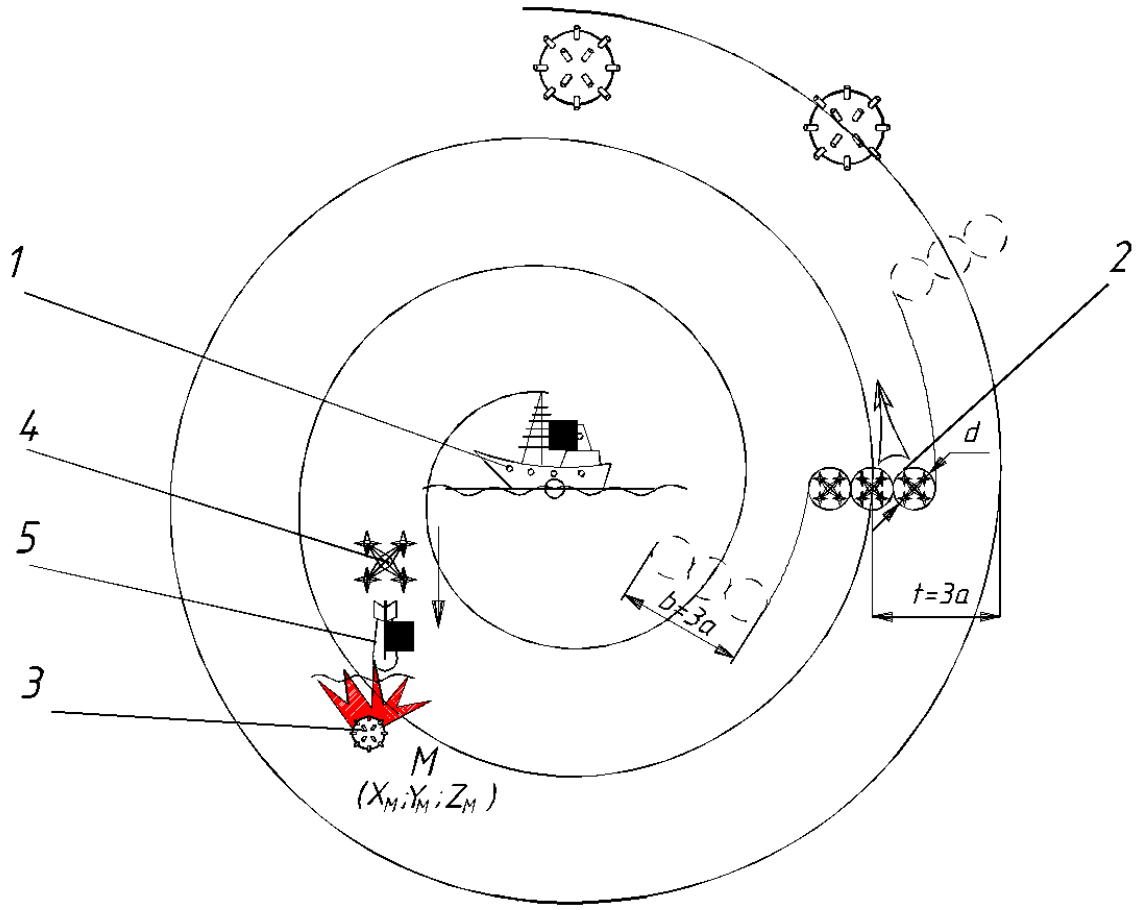

Source: Own development

Fig. 1: The trajectory of spatial movements of search drones along the Archimedean spiral

Search drones 2 arranged in one line are given a command to spatially move this trio of drones along an Archimedean spiral, whose pitch is equal to

$$b=3a=3d=6r,$$

where b=3a – the width of the area of simultaneous coverage of the search zone by the drones 2; d and r – diameter and radius of the hemisphere of the action of the search radar equipment respectively.

The center of the Archimedean spiral, along which the search drones move in the air, is conventionally arranged on the trawler boat 1, and the flight height does not exceed the radius r of the effective action of the search equipment. With the above parameters of search equipment, the following parameters of the flight path of search drones could be recommended as optimal:

- Flying height – 50 m;
- Distance between the drones – a=100 m;
- t=6r=6·50=300 m – pitch of the Archimedean spiral of spatial movement of the drones;
- r=50 m – radius of the hemisphere of the effective search of radar equipment;
- b=3a=3·100=300 m – the width of the search area covered by three drones.

The trajectory of the search drones 2 along the Archimedean spiral was chosen for two reasons:

- This trajectory does not allow the presence of unsurveyed areas of the sea water area;
- This smooth trajectory, unlike other possible ones, does not involve reverse movements and sharp turns, which is not desirable for aircraft.

If we take the speed of search drones as the average permissible flight speed v=5-5,5 m/s=18-20 km/h, then in one hour these three search drones will survey approximately six square kilometers of sea water area during their spatial movements along the Archimedean spiral.

In the event that any of the search drones 2 detect a floating mine, their Archimedean spiral flight over the territory is suspended. According to the appropriate command from the command post of the trawler boat 1, the drones 2 "hover" over the detected mine, locating above it in an equilateral triangle, the geometric center of which coincides with the point of placement of the mine 3 [6, 14].

After that, the observational identification equipment is turned on simultaneously on three drones to identify the object detected by the drones 2 on the sea surface. It is the observation and photos of a floating object from three points (drones) shifted 1200 from each other that make it possible to build a solid-state model of the object under study on computer screen. That is why exactly three search drones are used simultaneously in this mine search scheme.

If a floating object discovered on the surface of the sea turns out to be a floating mine, they proceed to its disposal. To do this, they first of all determine the coordinates of location of this mine using an appropriate computer program. This program involves the introduction of an imaginary system of orthogonal spatial Cartesian coordinates with the location of the origin of the coordinates at the location of the trawler boat 1 (Fig. 2). The x-axis is tentatively directed towards one of the geodetic sides of the world of the investigated mine search area, for example, to the south. The y-axis perpendicular to it is in the direction of the other side of the world, for example, to the east. The z-axis is directed upwards perpendicular to the other two axes. The horizontal plane of projections of this coordinate system formed by two mutually perpendicular x and y axes coincides with the surface of the sea.

The directions of the axes are assigned in such a way that the detected mine and search drones are located within the first octant of the space outlined by the projection planes (Fig. 2) [10].

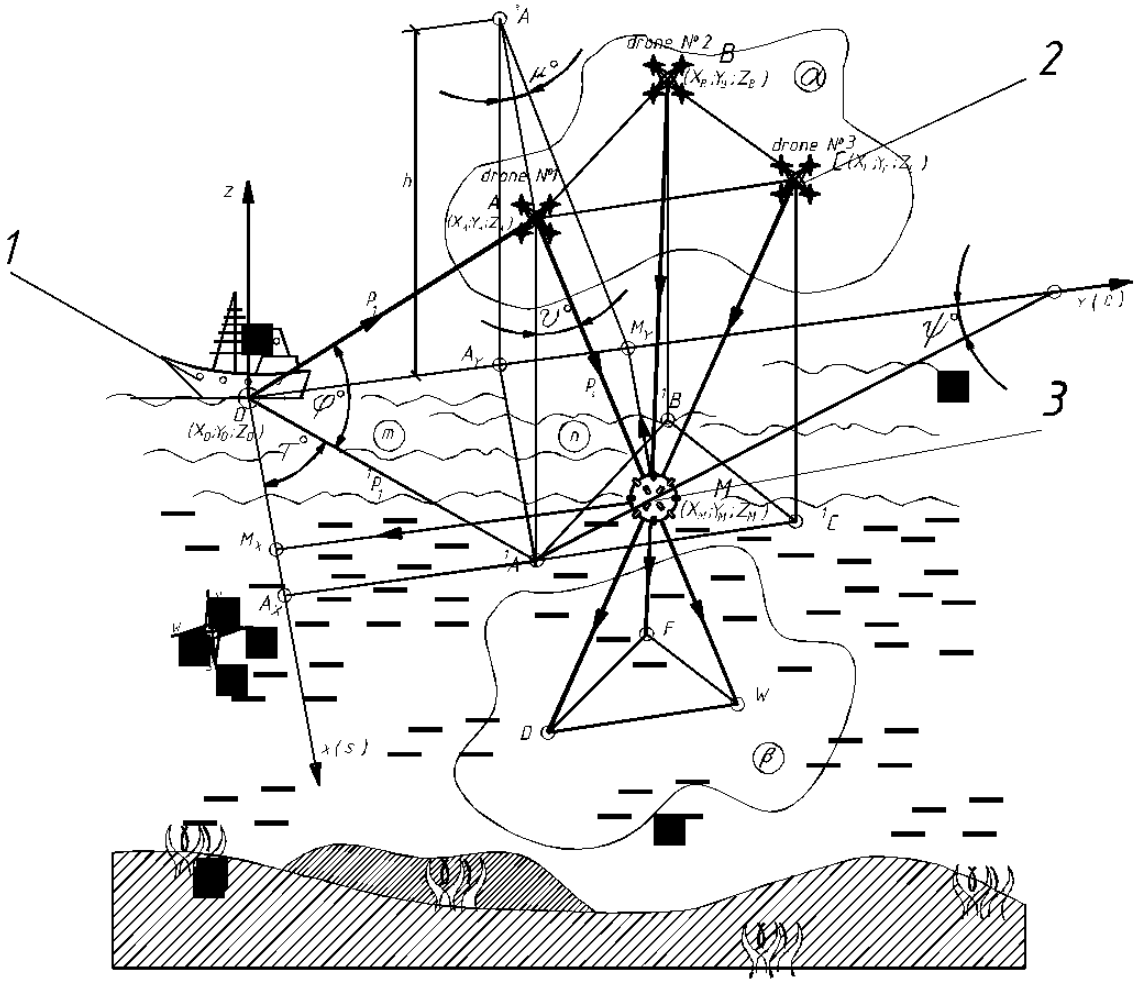

Fig. 2: Scheme for calculating the coordinates of a floating mine detected by search drones [10]

The radar station installed on the trawler 1 determines the coordinates of each drone placed over the mine 3 in the introduced system. These coordinates include the distance l from the radar to each of the three search drones 2 that are currently placed over the detected mine 3, as well as the angles of inclination of the imaginary projecting rays passing from the radar to each of the drones. In Fig. 2, these structures are marked as follows:

- Search drones N°1-A, N°2-B, and N°3-C, and their projections on the sea surface plane ^{1}A, ^{1}B, ^{1}C respectively;
- Distance from the radar station to the search drones l_1=OA; l_2=OB; l_3=OC;
- Projecting rays that pass from the radar station through the search drones– p_1, p_2, p_3. Their projections on the sea surface plane are $^1p_1$, $^1p_2$, $^1p_3$ respectively;
- Angles between projecting rays and their projections on the sea surface area respectively:

$$\varphi^\circ = p_1 \wedge {}^1p_1 = OA \wedge O^1A \text{ (Fig. 2);}$$
$$\gamma^\circ = p_2 \wedge {}^1p_2 = OB \wedge O^1B \text{ (Fig. 3);}$$
$$\delta^\circ = p_3 \wedge {}^1p_3 = OC \wedge O^1C \text{ (Fig. 4).}$$

Further calculations of the coordinates of the location of the detected mine are carried out using the appropriate software according to the following algorithm [6, 10].

First, from the respective triangles ΔAO^1A, ΔBO^1B, and ΔCO^1C, the height of the drones 2 above the sea surface $h=l_1\sin\varphi$ is determined and equalized for all the three drones. The plane formed by the three drones 2 is denoted as the base plane α (A, B, C). This base plane α is parallel to the sea

surface and is distant from it by the height $h = |\alpha\ ^1\Pi|$.

The calculation program further provides that imaginary projecting rays pass from the portable radar stations of the drones through the drones 2 themselves and the detected mine, that is p_4=AM, p_5=BM and p_6=CM. The angles of inclination of these projecting rays to the corresponding perpendiculars from points A, B and C to the surface of the sea plane are recorded:

$$\upsilon^o = p_4 \hat{}\ A\ ^1A = AM \hat{}\ A^1A;$$
$$\xi^o = p_5 \hat{}\ B\ ^1B = BM \hat{}\ B^1B;$$
$$\varepsilon^o = p_6 \hat{}\ C\ ^1C = CM \hat{}\ C^1C.$$

Below the sea surface, at the depth of $h_1 = \frac{h}{2}$, an imaginary so-called "picture" plane β is arranged by the calculation program parallel to the sea surface $^1\Pi(x, y)$ and the base plane α(A, B, C). The imaginary projecting rays p_4, p_5 and p6 that pass from the search drones through the detected mine M are continued to the intersection with the "picture" plane β and the coordinates of their intersection points are calculated, namely

$$W(x_W, y_W, z_W) = \rho_4 \cap \beta\ //^1\ \Pi;$$
$$F(x_F, y_F, z_F) = \rho_5 \cap \beta\ //^1\ \Pi;$$
$$D(x_D, y_D, z_D) = \rho_6 \cap \beta\ //^1\ \Pi.$$

At the same time, for spatial binding of projecting rays to the selected coordinate system, the angle of their inclination to any vertical projections plane of the selected coordinate system is additionally determined from the azimuths of the projecting rays determined by drone radars. For example, the profile plane 3P(y, z), formed by the intersection of the y and z axes. Then

$$\mu^o = p_4 \hat{}\ ^3\Pi\ ;\ \lambda^o = p_5 \hat{}\ ^3\Pi\ ;\ \chi^o = p_6 \hat{}\ ^3\Pi.$$

The two pyramids MABC and MWFD formed by projecting rays p_4, p_5 and p_6 and mutually parallel bases are similar. Their base planes α (A, B, C) and β (W, F, D) are mutually parallel. These pyramids have a common vertex at point M, where the detected mine is located. The angles of their corresponding faces at the vertex M are equal to each other, and the side edges of one pyramid are extensions of the edges of the other. Having the coordinates of points A, B and C at the base of the upper pyramid ABCM as measurement data of the trawler boat 1 radar station and the coordinates of points W, F and D at the base of the lower pyramid as measurement data of drone radars, it is possible to calculate the coordinates of the common top of these pyramids, i.e. point M as the point where the detected floating mine 3 is currently located.

The projecting ray p_1 that is tentatively directed from the the trawler boat 1 radar station towards drone 1 (point A in Fig. 2) and its projection $^1p_1$ onto the horizontal projections plane $^1\Pi$, as well as the connecting line between the points A and ^1A form the plane τ (ΔAO^{1}A) established by the triangle ΔAO^{1}A that is perpendicular to $^1\Pi$, i.e. τ (ΔAO^{1}A) ⊥ $^1\Pi(x, y)$. The radar station azimuth by the projecting ray p_1 allow establishing its inclination angle to $^1\Pi$, i.e. $\varphi^0 = OA \hat{}\ O^1A = p_1 \hat{}\ ^1p_1$ and clarifying the location height of drone 1 (point A) above the sea surface

$$z_A = h = A^1A = OA \cdot \sin\varphi = l_1 \cdot \sin\varphi,$$

where l=OA - the distance l_1 from the trawler boat to drone 1 determined by the radar station.

The length of the projections $^1p_1$ of the projecting ray p_1 on the horizontal projections plane is

$$^1p_1 = O^1A = OA \cdot \cos\varphi = l_1 \cdot \cos\varphi.$$

Then the coordinates of the points A and ^1A are determined from the right triangles Δ^1AOA_x and Δ^1AOA_y

$$x_A = OA_x = O^1A \cdot \cos\tau = l_1 \cdot \cos\varphi \cdot \cos\tau$$

$$y_A = A_x\ ^1A = OA_y = {}^1p_1 \sin\tau^0 = O^1A \cdot \sin\tau^0 = l_1 \cdot \cos\varphi \cdot \sin\tau$$

Here τ - the angle between $^1p_1 = O^1A$ and the x axis.

Therefore, all the location coordinates of drone 1 (point A), drone 2 (point B), and drone 3 (point C)

are determined in the selected coordinate system, namely:

$$x_A = l_1 \cdot \cos\varphi \cdot \cos\tau \;;\quad x_B = l_2 \cdot \cos\gamma \cdot \cos k \;;\quad x_C = l_3 \cdot \cos\delta \cdot \cos\eta \;;$$

$$y_A = l_1 \cdot \cos\varphi \cdot \sin\tau \;;\quad y_B = l_2 \cdot \cos\gamma \cdot \cos k \;;\quad y_C = l_3 \cos\delta \cdot \cos\eta \;; \qquad (1)$$

$$z_A = l_1 \cdot \sin\varphi \;;\quad z_B = l_2 \cdot \sin\gamma \;;\quad z_C = l_3 \sin d \;;$$

Here k° - the angle between the projection of the projecting beam ¹p_5 and axis x Fig. 3, and the angle η°- is the angle between the projection of the projecting beam ¹p_6 and axis x Fig. 4.

Using the portable radar, the projecting ray p_4 is visually directed from drone 1 located at point A to the detected mine lying on the surface of the sea at point M. In our case, in the selected coordinate system, point M, i.e. the detected mine, is placed on the horizontal projections plane ¹Π(x, y). Similarly to the previous case, the projecting ray p_4=AM was considered (Fig. 2). Its projection on ¹Π, i.e. ${}^1p_4 = M{}^1A \subset {}^1\Pi$ and the connecting line A¹A form a right triangle ΔAM¹A, whose plane π(ΔAM¹A) is perpendicular to the projections plane ¹Π. The plane of this triangle is inclined to the projections plane ${}^3\Pi(y,z)$ at an angle of ψ°. Using the azimuth of the drone 1 radar, the inclination angle of its imaginary projecting ray p_4 to the connecting line A¹A is determined, namely $\nu^0 = p_4 \hat{} A^1A$.

The length of the segment AM is determined from the right triangle ΔAM¹A

$$l_4 = AM = \frac{{}^1AA}{\sin\nu} = \frac{{}^1AA}{\sin\nu} = \frac{h}{\sin\nu}, \qquad (2)$$

and the difference between the coordinates of the points ¹A and M is determined from the right triangle ¹AMK, i.e.:

$$\Delta x_M = MK = {}^1AM \cdot \sin\varphi = h \cdot tg\psi \cdot \sin\varphi \;;$$
$$\Delta y_M = {}^1AK = {}^1AM \cdot \cos\varphi = h \cdot tg\psi \cdot \cos\varphi \;. \qquad (3)$$

Therefore, the coordinates of the located mine 3 (point M) in the selected coordinate system will have the following calculated values:

$$x_M = x_A \pm \Delta x_M = l_1 \cdot \cos\varphi \cdot \cos\tau \pm h \cdot tg\nu \cdot \sin\psi = h\left(\frac{\cos\tau}{tg\varphi} \pm tg\nu \cdot \sin\psi\right);$$
$$y_M = y_A \pm \Delta y_M = l_1 \cdot \cos\varphi \cdot \sin\tau \pm h \cdot tg\nu \cdot \cos\psi = h\left(\frac{\sin\tau}{tg\varphi} \pm tg\nu \cdot \cos\psi\right), \qquad (4)$$
$$z_M = 0 \;.$$

The "+" sign is used in the above dependencies if the φ angle is acute, and the "-" sign is used if the ψ° angle is obtuse. Thus, using a simple calculation program, on the basis of the data provided by the radar system installed on the trawler boat 1 and the data from portable radars on drones, the coordinates of the floating mine 3 detected by the drones 2 are determined.

To clarify the coordinates of the mine, the above calculations are duplicated for the other two drones. The initial data for these calculations and the calculation scheme are shown in Fig. 3 and Fig. 4.

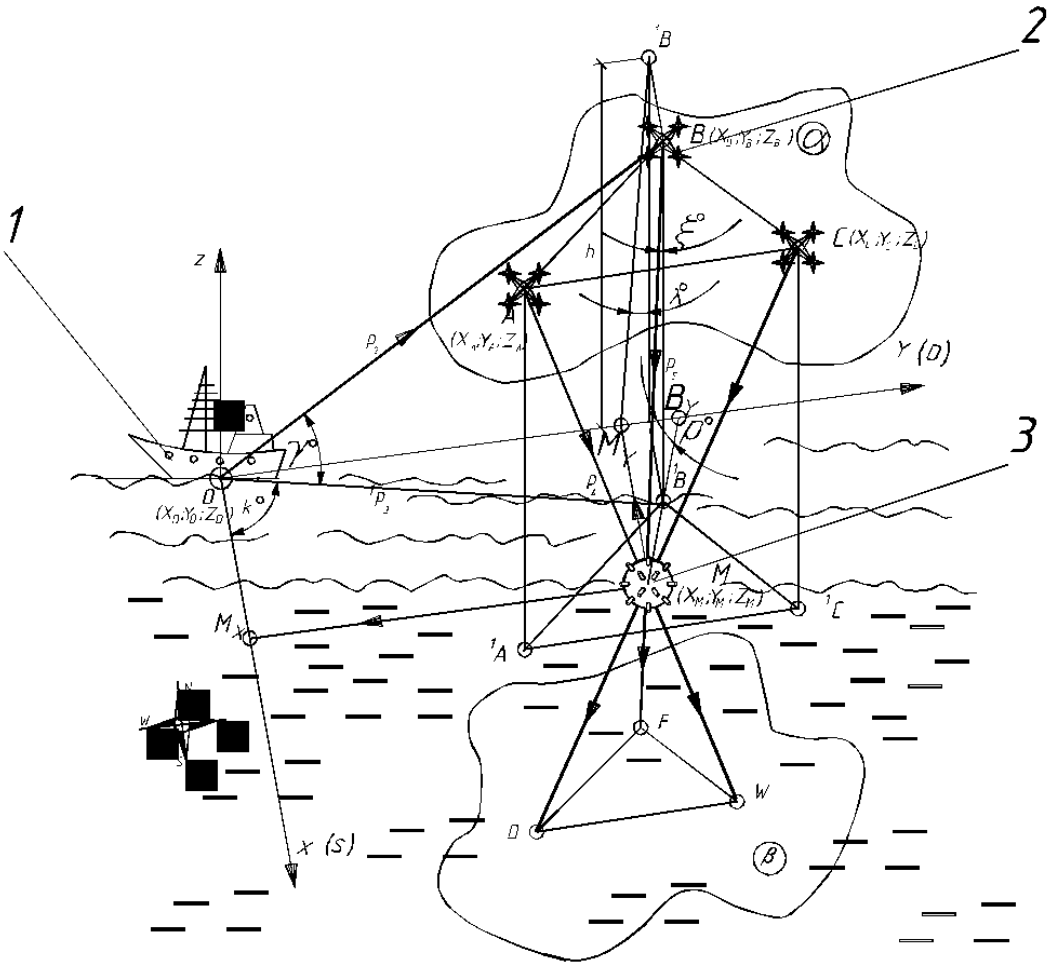

Source: Own development

Fig. 3: The scheme of specifying the coordinates of the found mine by drone N° 2 (point B)

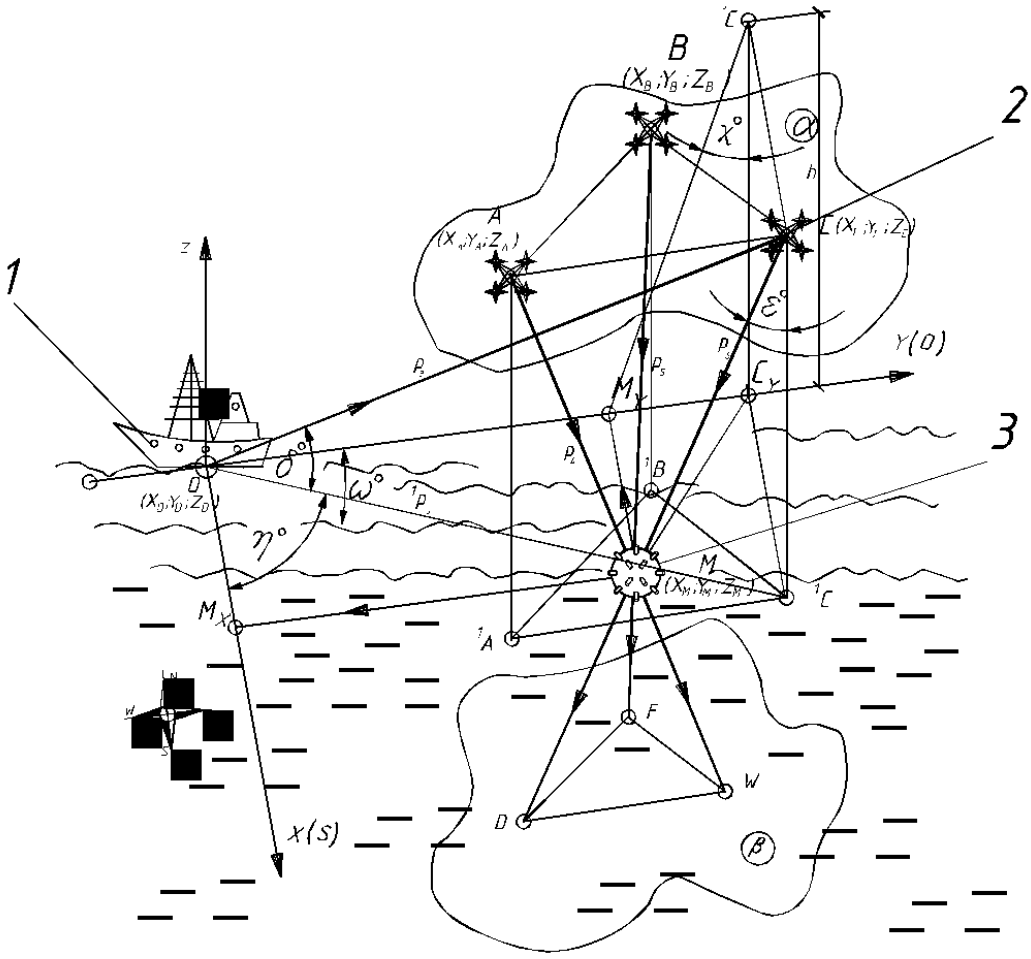

Source: Own development

Fig. 4: The scheme of specifying the coordinates of the found mine by drone N° 3 (point C)

In order to check the correctness of the calculations, the coordinates of the points W, F, and D are determined according to a similar scheme on the projecting rays p_4 , p_5 , p_6 that are located on the parallel base "picture" plane $\beta(W,F,D)$. Having the coordinates of the points at the ends of the segment of the projecting ray, one can write down the following equation of the straight line passing through the two points with known coordinates $A \in p_4;\quad A(x_A,y_A,z_A);$ $W \in p_4;\quad W(x_w,y_w,z_w);\quad p_4 \subset l_4$.

Then the equation of the straight lie l_4 will be as follows

$$\frac{x-x_A}{x_w-x_A}=\frac{y-y_A}{y_w-y_A}=\frac{z-z_A}{z_w-z_A}. \qquad (5)$$

Similarly, for the projecting ray p_5 passing through drone 2 (point B), the detected mine 3 (point M), and point F with known coordinates $F(x_F,y_F,z_F)$, the equation of the straight line l_5 passing through the projecting ray p_5 will be as follows

$$\frac{x-x_B}{x_F-x_B}=\frac{y-y_B}{y_F-y_B}=\frac{z-z_B}{z_F-z_B}. \qquad (6)$$

All the same constructions and calculations are made for the third ray passing through drone 3, mine M and point D on the "picture" plane. The equation of the straight line l_6 passing through these points will be the following:

$$\frac{x-x_C}{x_D-x_C}=\frac{y-y_C}{y_D-y_C}=\frac{z-z_C}{z_D-z_C}. \qquad (7)$$

Equation systems are formed from any two equations of projecting rays, and by their joint solution, the coordinates of points M, in which the detected mine 3 is located, are searched. If the detected coordinates of the point of intersection of the three projecting rays match in all the above-mentioned check steps, it may be concluded that the calculated coordinates of the mine correspond to their real value.

To neutralize the detected mine 3, the crew of the trawler boat 1 decides which available method of direct mine neutralization to use. Several options are possible, including mine detonation using a UAV. In this case, drone 4 available on the trawler boat is used. In the automatic holder of this drone 4, a corresponding warhead 5 is installed, the explosive substance of which is sufficient to detonate the detected mine. The liquidator drone carrying a warhead is given calculated coordinates of the detected mine 3 and is directed to liquidate the mine (Fig. 5).

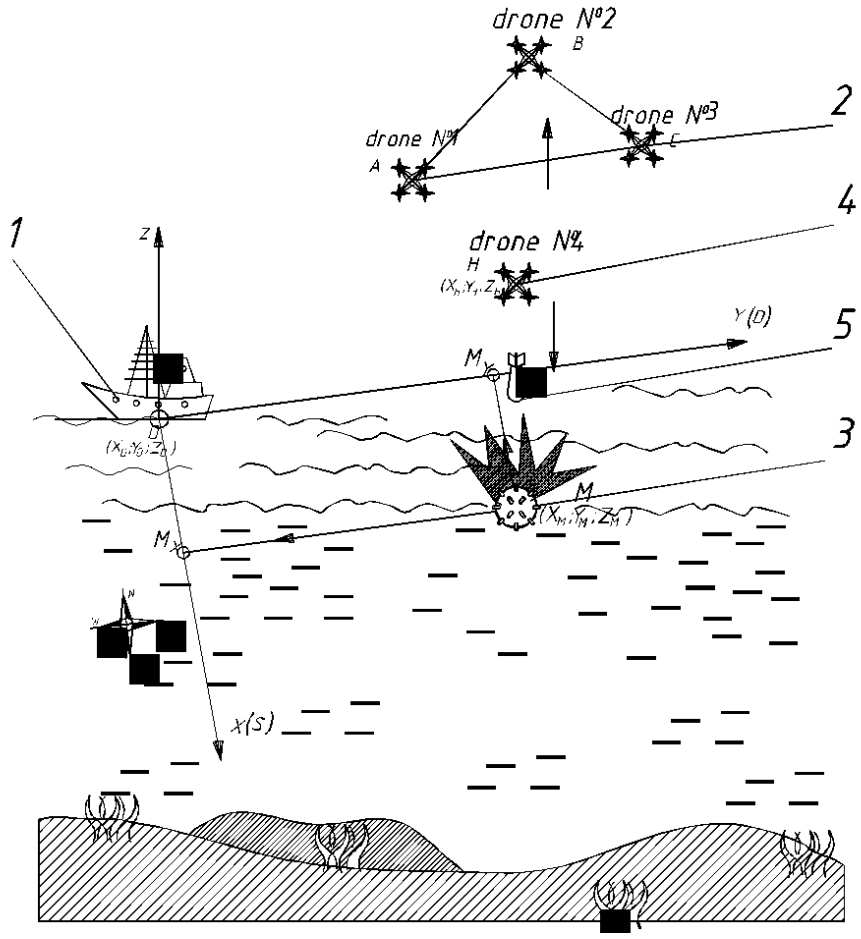

Source: Own development

Fig. 5: Liquidation of the detected floating mine

Search drones N°1, N°2, and N°3 rise to a safe height, the drone 4 that detonates a mine is located above the mine 3 and, if possible, once again checks the type of the mine with a video camera and waits for the command to take further actions. The command post finally analyzes the safety of mine 3 explosion for the environment, for people, and the search equipment and gives the command to detonate the mine. The launch mechanism of the liquidator drone 4 that detonates a mine unlocks the warhead 5 holder and the explosive charge falls directly on the mine 3 or next to it in the water. As a result of the explosive contact of the warhead with the mine or water, the warhead explodes, provoking the explosion of the detected mine 3 due to its mechanical damage or detonation of the explosive substance.

Figure 6 shows a block diagram for making calculations and building a computer program to

determine the coordinates of a floating mine detected by UAV. The calculation block diagram requires inputting some data, such as the model and number of search drones, characteristics of their spatial location and movement, flight height during the search for floating mines.

Tabular input data of the block diagram for calculating the coordinates of floating mines

Table 1

Item	Name of the given parameter	Designation and numerical value of the given parameter
1	Number of search UAV	UAV model - Number of UAV – 3
2	Trajectory of UAV search movements	Archimedean spiral Interturn distance or spiral pitch t = 3a=3·100=300 m, a =100 m – distance between drones
3	Search area band width	b=3a=3·100=300 m
4	UAV location at the time of mine detection	Triangle ABC with the length of each side a=100 m and angle 120° at vertexes
5	UAV location height above the detected mine	h=25–50 m

The calculation itself is completed in a few stages, namely calculating the distance between the base trawling boat to each drone placed above the mine, calculating the coordinates of projections of the search drones onto the sea surface, determining the length of the projecting rays generated by the drones onto the detected mine etc. Based on these data, mine coordinates are calculated, and their accuracy is checked. In case of discrepancies in the data calculated for each of the search drones, the angles of inclination and the length of the projecting rays of the trawler boat radar station and the similar data of the search drones are clarified (Fig. 5).

Parameters of projecting rays and their projections in the selected coordinate system (Fig. 2, Fig. 3, Fig. 4)

Table 2

Item	Projecting rays of the trawling boat radar station (Fig. 2)			
	Elements of the spatial arrangement of projecting rays and their projections	Drone 1	Drone 2	Drone 3
1	Length l_i of projecting rays	$p_1=l_1=OA$	$p_2=l_2=OB$	$p_3=l_3=OC$
2	Length of projections p_i of projecting rays	${}^1p_1={}^1OA$	${}^1p_2={}^1OB$	${}^1p_3={}^1OC$
3	Angles of inclination of projecting rays and their projections to the sea surface (horizontal projections plane ${}^1\Pi$); Angles of inclination of projections of the projecting rays p_i to the x axis	$\varphi=p_1\hat{}\,{}^1p_1$ $\tau={}^1p_1={}^1OA$	$\gamma=p_2\hat{}\,{}^1p_2$ $k={}^1p_2={}^1OB$	$\delta=p_3\hat{}\,{}^1p_3$ $\eta={}^1p_3={}^1OC$
	Projecting rays and their projections generated by search drones (Fig. 3, Fig. 4)			
	Elements of spatial arrangement of projecting rays and their projections	Drone 1	Drone 2	Drone 3
4	Length l_i of projecting rays of the drones	$p_4=l_4=AM$	$p_5=l_5=BM$	$p_6=l_6=MC$
5	Length of projections p_i of projecting rays of the drones	${}^1p_4={}^1MA$	${}^1p_5={}^1MB$	${}^1p_6={}^1MC$
6	Angles of inclination of projecting rays and their projections to the vertical connecting line	$\nu=p_4\hat{}\,{}^1A$	$\xi=p_5\hat{}\,{}^1B$	$\varepsilon=p_6\hat{}\,{}^1C$
7	Angles of inclination of the planes passing through projecting rays perpendicular to the sea surface to the projections plane ${}^3\Pi$	$\psi=n_4\hat{}\,{}^3\Pi$	$\rho=n_5\hat{}\,{}^3\Pi$	$\omega=n_6\hat{}\,{}^3\Pi$
8	Angles of inclination of projecting rays to the profile projections plane ${}^3\Pi$	$\mu=p_4\hat{}\,{}^3\Pi$	$\lambda=p_5\hat{}\,{}^3\Pi$	$\chi=p_6\hat{}\,{}^3\Pi$

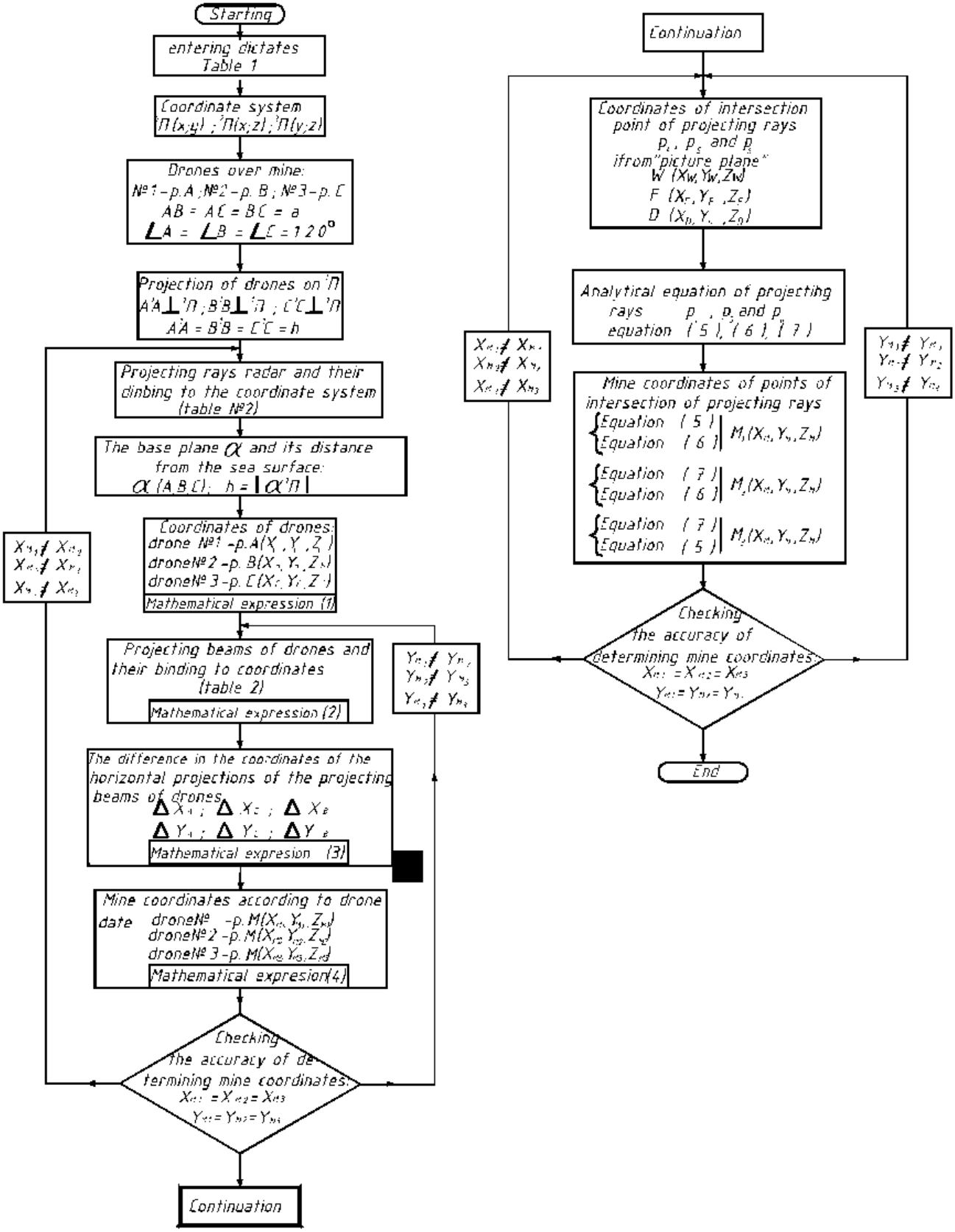

Source: Own development

Fig. 6: Block diagram for calculating the coordinates of detected floating mines.

Thus, when using this method of searching for and neutralizing mines, there is practically no need for people in the command post of the trawler boat to come into direct contact with a

life-threatening mine. However, demining situations can be different, of course. For example, the power of the warhead dropped from a liquidator drone may not be enough to detonate a mine. Then the trawler boat will have to trawl the area of the sea where the mine is located or use other more powerful means of neutralizing mines such as, for example, floating drones equipped with guided destroyer torpedoes or the so-called kamikaze robots. Their self-detonation on a detected mine destroys its shell and the mine either explodes or collapses, ceasing to be a threat to people and vessels.

IV. DISCUSSION

Like most engineering solutions, the proposed method of demining seas and rivers has both advantages and disadvantages. Arguably the most significant drawback is that it is only suitable for floating mines drifting on water surface. It is not suitable for demining the so-called anchor mines nor for neutralizing bottom mines because portable radars equipped with search drones cannot effectively scan the water layer in which these mines are located.

Another noticeable disadvantage of the proposed demining method is its critical dependence on weather conditions. Winds with a speed of more than 7-8 m/s, waves 1.5 meters high, excessive smog in the air, intense rain or snowfall – all these conditions make using drones impossible, and, accordingly, make it impossible to use kinematic projection for locating mines on the sea surface.

A certain disadvantage is that mines detected by this method cannot be deprived of buoyancy or fixed at the place of their detection. Therefore, these detected floating mines must be neutralized immediately upon detection. Otherwise, they may be carried away by winds or currents to other areas and search for them will have to be started again.

On the other hand, there are two undeniable advantages to the method of using kinematic projection for detecting floating mines. First of all, it is complete elimination of people both from searching and demining. This is very important, because the demining process is not only long-term, but also extremely dangerous for the trawler crew and divers.

Another significant advantage of this demining method is relatively high productivity and speed of search operations [14]. Wide area coverage by three drones and their coordinated movements along the Archimedean spiral contributes to effective search operations. The method eliminates the presence of unsurveyed areas, which are rather common during round-trip movements of search vessels.

Another important positive aspect is minimized search movements of the trawler. It either stands at anchor or drifts with minimal consumption of fuel by the propulsion engines. Undeniably, this compensates for the costs of purchasing search equipment for drones and creating software for managing search movements of the drones. After all, in order to patrol a sea area of 6 km^2, a boat would have to sail about 20 kilometers an hour, spending about 20 liters of fuel worth about 1,000 hryvnias, and there will be at least 5-6 such plots during one working day, therefore it is a daily saving of 5-6 thousand hryvnias.

Unfortunately, given the military events on the territory of Ukraine, the authors of the article were unable to carry out field tests of the proposed demining scheme. The authors hope to do this in the future in peacetime and invite all individuals and organizations interested in the results of this research to cooperate.

V. CONCLUSIONS

1. The rapid development of science and technology at the turn of the millennium significantly improved military weapons in general and means of mining both on land and in water in particular. The latest technologies of manufacturing explosives, modern materials used for the manufacture of mines, high-quality electronics for controlling the moment of explosion, and other achievements have turned modern mines from a “passive bystander” into powerful hyperactive autonomous destroyers of water vehicles.

2. Among various types of mine weapons used in the water areas of rivers and seas, floating mines are the least powerful. However, they are the most insidious due to the lack of controllability of their movements by winds, currents, and waves. Therefore, along with the danger to military vessels, these mines are even more dangerous to the civilian population living, working or resting on the shore. Having drifted to the shore or hitting coastal rocks, this mine suddenly explodes even from a shock contact with the soil or stones.
3. The essence of the proposed method is to use a group of UAV of the drone type to search for floating mines, the results being reduced to the calculation of the coordinates of the detected floating mine by means of kinematic projection. The use of small, economical search aircraft eliminates the need for search movements of trawler boats. This significantly reduces the cost of search operations and increases their safety for the trawler crew.
4. From among all the possible trajectories of movement of UAV and trawlers when searching for floating mines, three drones arranged in a row along an Archimedean spiral with an interturn step proportional to the number of search drones and the radius of effective action of their search equipment is recommended as the optimal flight trajectory.
5. Despite certain disadvantages of the method of searching for floating mines using kinematic projection, such as increased sensitivity to weather conditions, especially wind, this method has the prospect of wide practical application, mainly due to elimination of people's contact with the mine and elimination of movements of the trawler boat, thereby significant fuel saving, as well as high accuracy.

REFERENCES

1. Antonov R. BPLA dopomozhut vyjavyty nezdetonuvavshi bojeprypasy. 8 sichnja 2020. https://mil.in.ua/uk/news/bpla-dopomozhut-vyyavlyaty-nezdetonuvavshi-boyeprypasy/
2. Vertolitnyj tral na pidvodnyh krylah Harris MK-105 Foto: www.thinkdefence.co.uk.
3. Lavrivskyj M.Z., Tur N.Je. Vykorystannja bezpilotnyh litalnyh aparativ v monitoryngu nadzvychajnyh sytuacij u lisovij miscevosti – Naukovyj visnyk NLTU Ukrainy – 2015.- Vyp. 258. –S. 353-359.
4. Kucherenko Ju.F., Naumenko M.V., Kuznjecova M.Ju. Analiz dosvidu zastosuvannja bezpilotnyh lital'nyh aparativ ta vyznachennja naprjamku ih podalshogo rozvytku pry provedenni merezhecentrychnyh operacij. – Systemy ozbrojennja i vijskova tehnika, March 2018. DOI:10.30748/ soivt.2018.53.03.
5. Bespylotnaja razvedыvatelnaja avyacyja stran myra: ystoryja sozdanyja, opt boevogo prymenenyja, sovremennoe sostojanye, perspektyvы razvytyja: monogr /S.P.Mosov. – K.: Yzd.Dom. «Rumb», 2008.-160p.
6. Svidrak I.G., Shevchuk L.I., Strogan O.I., Strutynska L.R., Strogan I.V. Kinematychne proecijuvannja jak zasib upravlinnja tehnikoju v avtomatyzovanyh zemlerobnyh kompleksah // Naukovyj visnyk NLTU Ukrainy: zbirnyk naukovo-tehnichnyh prac. – 2021. – T. 31, № 5. – P. 102–107.
7. Aftanaziv I.S., Strogan O.I., Strutyns'ka L.R., Strogan I.V. Zastosuvannja kinematychnogo proecijuvannja v avtomatyzovanyh zemlerobnyh kompleksah комплексах // Problems of science and practice, tasks and ways to solve them : abstracts of XI International scientific and practical conference, Warsaw, Poland, March 22–25, 2022. – 2022. – P. 351–355.
8. Svidrak I.G., Baranecka O.R., Topchij V.I., Shevchuk A.O., Galkina N.S. Vyznachennja prostorovyh koordynat tochok panoramnogo znimannja. Zbirnyk nauk. prac MDPU im. B.Hmelnyckogo. m. Melitopol: Vydavnyctvo MDPU im. B.Hmelnyckogo, 2014.- Vyp. 2. - P. 136-140.
9. Shulc R.V., Vojtenko S.P., Krelshtejn P.D.,Malina I.A. Do pytannja rozrahunku tochnosti vyznachennja koordynat tochok pid chas aerofotoznimannja z bezpilotnyh litalnyh aparativ. Inzhenerna geodezija, 2015. Vyp. (62). P. 124–136.
10. Svidrak I.G., Aftanaziv I.S., Shevchuk L.I., Strogan O.I. Determination of coordinates of

unmanned aircrafts by means of kinematic projection // Mathematical Modeling and Computing. – 2022. – Vol. 9, № 2. – P. 459–469.
11. Svidrak I.G., Aftanaziv I.S., Strogan O.I., Shevchuk A.O. Kinematychne proecijuvannja v suchasnyh tehnologijah // Naukovyj visnyk Lvivskogo nacionalnogo universytetu veterynarnoi medycyny ta biotehnologij imeni S.Z. Gzhyckogo. Serija "Harchovi tehnologii". – 2021. – T. 23, № 96. – P. 67–75.
12. Aftanaziv I.S., Svidrak I.G., Strogan O.I. Vyznachennja koordynat bezpilotnyh litalnyh aparativ //Suchasni doslidzhennja u svitovij nauci: materialy II-i Mizhnarodnoi naukovo-praktychnoi konferencii (Lviv, 15-17 travnja, 2022 r.). – 2022. – P. 380–388.
13. Janchuk R.M., Trohymec S.M. Stvorennja kartografichnoi osnovy dlja rozrobky generalnyh planiv naselenyh punktiv za materialamy aeroznimannja z neprofesijnyh BPLA. Serija Tehnichni nauky, 2017. Vyp. 1 (77). P. 32–39.
14. V. Glotov, M. Fys, O. Pashhetnyk. Rozrobka metodyky pidvyshhennja tochnosti vyznachennja prostorovyh koordynat tochok objektiv pry aeroznimanni z BPLA Geodezija, kartografija i aerofotoznimannja. Vyp. 92, 2020 – P. 45-54.
15. O.P. Kalynovskaja, V.V. Glogovskyj, Y.G. Pulkevych. K probleme edynoj teoryy proekcyonnyh otobrazhenyj // Prykl. geom. y ynzh. graf. – Vyp. 57 – 1994, P. 45-50.

Effectiveness of Silica Fume as a Partial Cement Replacement in Recycled Aggregate Concrete

Md. Rejoan Chowdhury, Md. Mehedi Hasan, Md. Shakil Howladar, Mosaddek Billah, Md. Sabbir Hossen Shahin & Rasel Shikder

University of Global Village

ABSTRACT

Recycled concrete aggregate (RAC) can be used in structural concrete to lessen the environmental impact of waste concrete and the use of natural resources. The current study summarized the mechanical performances of concrete and assessed the synergistic impacts of recycled aggregate, likely at 100% content, with silica fume (SF) partially substituting cement. The study's primary variables included the dosage of silica fume used as a partial replacement of ordinary Portland cement (OPC) at five different percentages: 0%, 4%, 8%, 12%, and 16% by weight. Five distinct mixtures, designated RACSF-0, RACSF-4, RACSF-8, RACSF-12, and RACSF-16, were made using differing concentrations of silica fume for M30 concrete. The workability of concrete mixes was examined using the slump test.

Keywords: recycled aggregate concrete; silica fume; workability; compressive strength; splitting tensile strength.

Classification: DCC Code: 666.972

Language: English

Great Britain Journals Press

LJP Copyright ID: 392924
Print ISSN: 2631-8474
Online ISSN: 2631-8482

London Journal of Engineering Research

Volume 25 | Issue 2 | Compilation 1.0

Effectiveness of Silica Fume as a Partial Cement Replacement in Recycled Aggregate Concrete

Md. Rejoan Chowdhury[α], Md. Mehedi Hasan[σ], Md. Shakil Howladar[ρ], Mosaddek Billah[Ↄ], Md. Sabbir Hossen Shahin[¥] & Rasel Shikder[§]

ABSTRACT

Recycled concrete aggregate (RAC) can be used in structural concrete to lessen the environmental impact of waste concrete and the use of natural resources. The current study summarized the mechanical performances of concrete and assessed the synergistic impacts of recycled aggregate, likely at 100% content, with silica fume (SF) partially substituting cement. The study's primary variables included the dosage of silica fume used as a partial replacement of ordinary Portland cement (OPC) at five different percentages: 0%, 4%, 8%, 12%, and 16% by weight. Five distinct mixtures, designated RACSF-0, RACSF-4, RACSF-8, RACSF-12, and RACSF-16, were made using differing concentrations of silica fume for M30 concrete. The workability of concrete mixes was examined using the slump test. After increasing the proportion of SF, a declining trend was observed in the test results. The mechanical characteristics of RACSF were examined at 7 and 28 days using compressive and splitting tensile tests. The results demonstrated that adding SF enhanced RACSF's performance at both early and later curing ages, with the highest results occurring at 12% SF addition. As a result, it is advised to partially substitute 12% SF for cement in RAC.

Keywords: recycled aggregate concrete; silica fume; workability; compressive strength; splitting tensile strength.

Author α: Lecturer, Department of Civil Engineering, University of Global Village, Barishal, Bangladesh.

σ ρ Ↄ ¥ §: Undergraduate Student, Department of Civil Engineering, University of Global Village, Barishal, Bangladesh.

I. INTRODUCTION

A major step toward sustainable construction, recycled aggregate concrete (RAC) addresses the growing global concerns about the depletion of natural resources and the increasing amounts of construction and demolition waste (CDW). The total produced amount of CDW worldwide is approximately 3 billion tons per year, which not only pollutes the ecological environment but occupies a large amount of land resources [1]. In the meantime, conventional concrete production uses a lot of virgin aggregates, which are usually taken from riverbeds and quarries. This causes both ecological disruption and environmental deterioration. RAC, on the other hand, uses aggregates made from processed construction and demolition waste, which has two advantages: it reduces the environmental effect of waste disposal and preserves the depleting natural aggregate supplies [2]. Nevertheless, there are inherent difficulties in using recycled aggregates in the manufacturing of concrete. When compared to natural aggregates, recycled aggregates which are made of crushed concrete, often have unique properties. The presence of adhered mortar, a remnant of the original concrete mix, results in increased porosity, higher water absorption, and a greater tendency for crushing. These factors can compromise the mechanical properties and durability of RAC, leading to reduced strength, increased permeability, and heightened susceptibility to deterioration [3]. In response to these challenges, extensive research has been undertaken to enhance the performance of RAC. One promising avenue involves the incorporation of supplementary cementitious materials (SCMs), which serve as partial replacements for Portland

cement. Among the various SCMs explored, silica fume (SF) has garnered considerable attention due to its exceptional pozzolanic and micro-filling properties [4]. A highly reactive amorphous silica, silica fume is a byproduct of the manufacturing of silicon and ferrosilicon alloys [5]. Its exceptional capacity to improve the qualities of concrete is a result of its incredibly fine particle size, which is usually several times smaller than cement particles. Silica fume, when added to RAC, engages in pozzolanic interactions with the calcium hydroxide (CH) that is liberated during cement hydration. A denser and more precise microstructure results from this reaction, which also forms more calcium silicate hydrate (C-S-H) gel, the main binding phase in concrete.

The addition of silica fume to RAC gives a plethora of benefits. Firstly, it improves the strength and durability of the concrete [6]. Greater C-S-H gel synthesis strengthens the link between the recycled aggregates and the cement matrix, increasing the material's tensile, flexural, and compressive strengths. Secondly, silica fume decreases RAC's permeability, increasing its resistance to water and hostile chemicals like sulfates and chlorides. The long-term endurance of RAC structures is greatly increased by this increased impermeability, which shields them against deterioration and corrosion. In addition, utilizing silica fume in concrete results in a finer pore structure, which reduces the possibility of the alkali-silica reaction (ASR), a harmful occurrence that can cause concrete to expand and break. Through the mitigation of RAC's inherent limitations, silica fume facilitates the further use of this eco-friendly material in a range of structural applications. In addition to encouraging waste reduction and resource conservation, this strategy aids in the creation of concrete infrastructure that is more durable and resilient. A recent study expressed, addition of 10% SF increased both compressive and splitting tensile strength of RAC. Meanwhile the decreasing trend of strength was found for 15% SF content [3]. Another study revealed that after 28 days, compressive strength increased by 8.5% to 24% and tensile strength improved by 15% to 49.43% due to the addition of 12% SF in RAC [7]. So, this research aims to observe the mechanical performance of concrete having 100% RAC and an optimal percentage of SF which can be used as the partial replacement of cement. Alongside usage of recycled aggregate concrete with silica fume is expected to become more significant in determining the direction of building and construction in the future as the industry looks for sustainable alternatives, recycling of materials, and ensure long term cost effectiveness of structures [8-9].

II. MATERIALS AND METHODS

2.1 Materials

In this study, locally available 43G Ordinary Port and Cement (OPC) was used. The coarse material used in this investigation was gathered from nearby vendors. In this investigation, recycled coarse aggregate with a maximum particle size of 20 mm was taken from crushed concrete slabs that had been removed. Also, Sylhet sand was collected from the local market. Table 1 shows the results of the property tests for coarse recycled stone and fine aggregate [10].

Table 1: Properties of Fine and Coarse Aggregate

Properties	Fine aggregate (FA)	Coarse aggregate
Fineness modulus	2.61	7.31
Specific gravity	2.63	2.78
Moisture content (%)	1.83	2.01
Loose density (kg/m3)	1465	1457
Bulk density (kg/m3)	1555	1572
Void ratio (%)	40.75	43.33

Silica fume was collected from the local supplier. An ultrafine powder has been collected as a byproduct of the manufacture of silicon and ferrosilicon alloys. The chemical compositions of the OPC and silica fume are shown in Table 2.

Table 2: Chemical Composition of OPC and Silica Fume

Constituents	Weight of OPC (%)	Weight of Silica fume (%)
SiO_2	19.01	89.94
Al_2O_3	4.58	0.51
Fe_2O_3	3.20	0.65
CaO	66.89	0.75
MgO	1.26	1.52
Na_2O	1.205	0.21
MnO	0.19	-
K_2O	2.76	0.47
SO_2	0.45	0.09

2.2 Mix Design of Concrete

Concrete mix proportions of 1: 1.90: 2.50 (Cement: FA: CA), water to cement ratio (W/C) 0.46 were obtained and was utilized for making M30 concrete according to the ACI 211.1-91. The process of concreting works was performed manually conforming ASTM C685 guidelines. Silica fume was used as a cement substitute led to different concrete mix designations at the rate of 0%, 4%, 8%, and 16%. Five concrete mixes have been done with respect to the silica fume percentage variation shown in Table 3. The reference mix was done with 0% silica fume and identified as RACSF-0, and the other mixes were identified as RACSF-0, RACSF-4, RACSF-8, RACSF-12, and RACSF-16. Requisite materials per cubic meter concrete are detailed below in Table 3.

Table 3: Details of Concrete Mix Design

Specimen type	Cement (Kg/m^3)	Water (L)	W/C	Fine aggregate (Silica sand) (Kg/m^3)	Coarse aggregate (Recycled stone) (Kg/m^3)	Silica fume (%)
RACSF-0	386	185	0.46	762	1006	0
RACSF-4	371	185	0.46	762	1006	4
RACSF-8	355	185	0.46	762	1006	8
RACSF-12	340	185	0.46	762	1006	12
RACSF-16	325	185	0.46	762	1006	16

2.3 Tests on Concrete

2.3.1 Workability Test

This test was carried out using slump cone, plate and tamping rod by following ASTM C143 [11]. Workability test shows the impact of silica fume on slump value of concrete.

2.3.2 Compressive Strength Test

This test was performed by following ASTM C140. Three cubes having standard size of 150 mm x 150 mm x 150 mm were required for each percentage of silica fume [12]. Saving cost and easy working process were major concerns regarding the selection of cubical specimens.

2.3.3 Splitting Tensile Strength Test

According to the ASTM C496 standard, the cylinder specimen used in this investigation underwent split tensile testing.

III. RESULTS AND DISCUSSIONS

3.1 Workability of Concrete: Slump Test

The changes in slump values with the addition of silica fume in RAC are demonstrated in Figure 3. Silica fume significantly reduces the slump of recycled aggregate concrete. This happens because silica fume particles are extremely fine and possess a very large surface area. From the graphical representation, it is seen that the slump values decrease with the increase in silica fume percentages from 79 mm to 64 mm. Relevant works have also shown that adding silica fume to concrete causes slump values to decrease [13]. Due to the cementitious qualities, silica fume binds the components of concrete together and is the primary reason why slump value decreases. Similar type of decreasing trend is found in concrete made with recycled aggregate and steel fiber [14-15]. The processing of recycled aggregate also increases surface roughness, which tends to reduce slump value and flow characteristics. More precisely, the rough texture and irregular shape of RACSF may cause resistance mobility and grain locking in concrete.

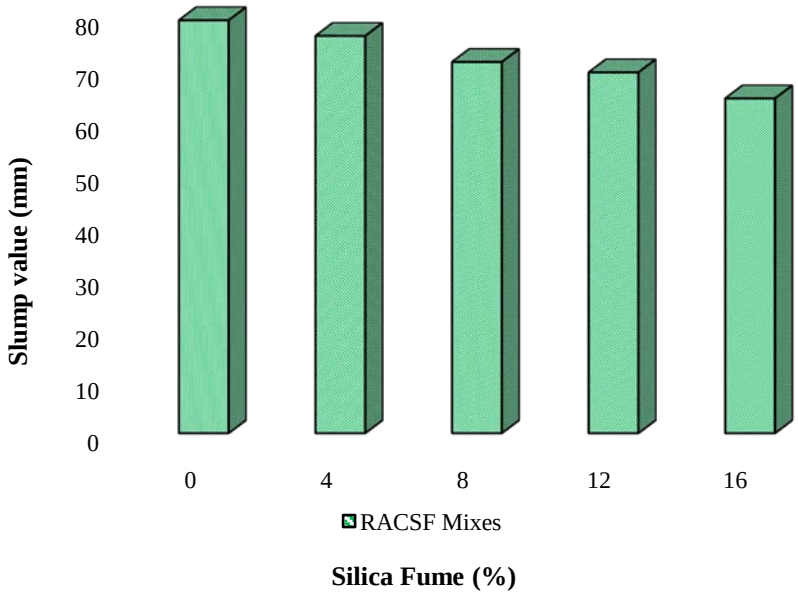

Figure 1: Fluctuation of Slump Based on Silica Fume Content

3.2 Impact of Silica Fume on Compressive Strength of Concrete

Table 4 summarizes the compressive strength test results of concrete mixes in terms of the mean strength, standard deviation, and lower and greater range of 95% confidence intervals.

Table 4: Summary of the Compressive Strength Test Result

Mixes	Days	Mean strength (MPa)	Standard Deviation, σ	95% confidence interval	
				Lower range	Upper range
RACSF-0	7	19.82	0.110	19.66	19.98
	28	30.12	0.144	29.95	30.29
RACSF-4	7	20.39	0.069	20.34	20.44
	28	30.38	0.116	30.12	30.64
RACSF-8	7	20.69	0.024	20.62	20.76

	28	31.27	0.137	30.97	31.57
RACSF-12	7	21.77	0.185	21.32	22.22
	28	32.87	0.198	32.47	33.27
RACSF-16	7	21.81	0.175	21.52	22.10
	28	31.49	0.076	31.38	31.60

Three specimens were tested in the laboratory for each silica fume concentration, and mean values were computed to obtain the final test results for compressive strength at 7 and 28 days. According to statistical analysis, the compressive strength fluctuated from 19.82 MPa to 31.49 MPa. Alongside, the standard deviation of tested specimens ranges from 0.024 to 0.198. The lowest compressive strength was 30.12 MPa with a 95% confidence interval bound of 29.95 MPa to 30.29 MPa and the highest compressive strength was 32.87 MPa with a 95% confidence interval bound of 32.47 MPa to 33.27 MPa. Furthermore, a standard deviation of strength less than 1 MPa indicates that the concreting work for this study was done with satisfactory quality control, because a deviation of up to 1.3 MPa indicates that the degree of quality control of concreting work complies with the laboratory precision according to the code of ACI [10]. Figure 3 simply visualizes the variation of mean compressive strength of RACSF specimens at 7 days and 28 days of curing.

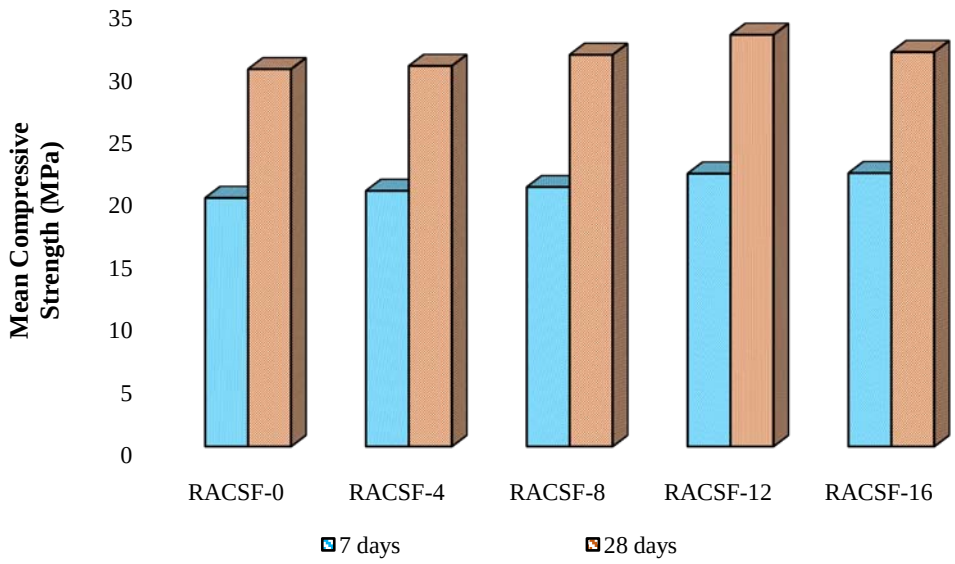

Figure 2: Compressive Strength Test Results of Racsf Mixes At 7 and 28 Days

Figure 3 illustrates how well the concrete created from silica fume and reclaimed stone worked by providing the necessary strength. The mean compressive strength of RACSF specimens was found to rise steadily up to 12% substitution of cement by silica fume. Concrete's compressive strength began to decline when the replacement level reached 16%. Therefore, after 7 and 28 days of curing, the investigation unequivocally showed that recycled aggregate concrete containing a certain amount of silica fume had a better compressive strength than control concrete specimens. A recent work shown that the strength increased with age for concrete that was younger than 28 days and peaked at 2 percent for concrete that was older. When the RA replacement was 50%, the compressive strength of RAC decreased with a low nano-silica (NS) concentration of 1%. NS improved the compressive strength of RAC at early curing ages for a 100% RA substitution [16].

Figure 4 shows that at 28 days, silica fume concentrations of 12% result in a more gradual percentage change in the compressive strength of RACSF in comparison to the control specimen. By adding silica fume of 12%, the compressive

strength is improved by up to 9.13%. While using 16% SF content, compressive strength increasing rate went downward at 4.55%. To comprehend the effect of silica fume substitution, the outcome is contrasted with a linear trend. A recent work indicated that the inclusion of silica fume at about 5 to 25% in concrete increases its compressive strength from 6% to 30% [17]. So, after taking into account the 28-day compressive strength test, the 12% incorporation rate of silica fume is decided to be optimal.

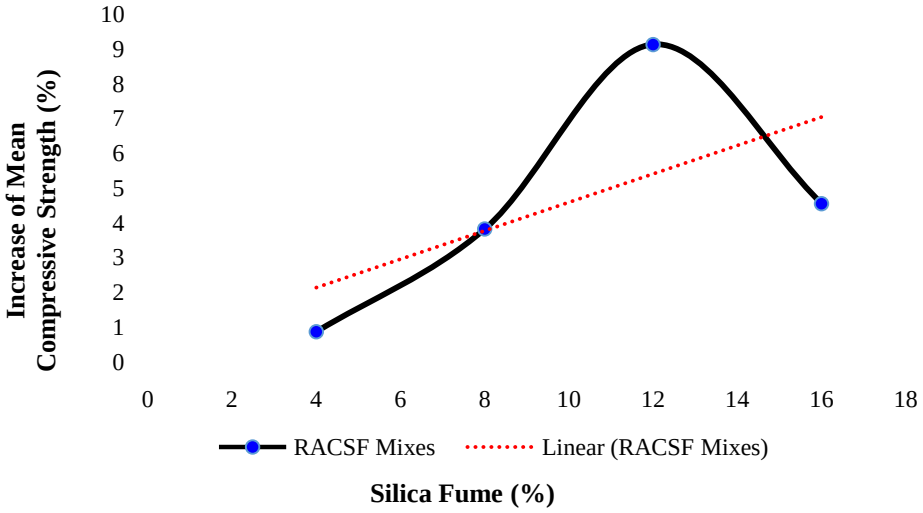

Figure 3: Percentage Increase of Compressive Strength 28 Days

3.3 Impact of Silica Fume on Splitting Tensile Strength of Concrete

After completing the splitting tensile strength test, Table 4 summarizes the test results of concrete mixes in terms of the mean strength, standard deviation, and lower and greater range of 95% confidence intervals.

Mixes	Days	Mean strength (MPa)	Standard Deviation, σ	95% confidence interval	
				Lower range	Upper range
RACSF-0	7	1.55	0.017	1.53	1.57
	28	2.67	0.056	2.57	2.77
RACSF-4	7	1.65	0.044	1.56	1.74
	28	2.83	0.025	2.74	2.92
RACSF-8	7	1.74	0.047	1.64	1.84
	28	3.13	0.040	2.93	3.33
RACSF-12	7	1.88	0.081	1.72	2.04
	28	3.37	0.059	3.19	3.55
RACSF-16	7	2.04	0.127	1.84	2.24
	28	3.22	0.023	3.09	3.35

Three specimens were tested in the laboratory for each silica fume concentration, and mean values were computed to obtain the final test results for compressive strength at 7 and 28 days. The splitting tensile strength fluctuated from 1.55 MPa to 3.37 MPa. Alongside, the standard deviation of tested specimens ranges from 0.017 to 0.127. The lowest tensile strength was 2.67 MPa with a 95% confidence interval bound of 2.57 MPa to 2.77 MPa and the highest tensile strength was 3.37 MPa with a 95% confidence interval bound of 3.19 MPa to 3.55 MPa. Moreover, a standard deviation of strength less than 1 MPa indicates that the concreting work for this study was done with

satisfactory quality control, according to the code of ACI. Figure 4 simply visualizes the variation of mean splitting tensile strength of RACSF specimens at 7 days and 28 days of curing.

The visualization of Figure 5 shows that the concrete made from recycled stone and silica fume performed well according to expectation. It was noticed that mean tensile strength of RACSF specimens increased gradually up to 12% replacement of cement by silica fume. When the replacement level was 16%, the tensile strength of concrete started to decrease. As a result, the study showed that recycled aggregate concrete with certain percentage of silica fume had higher strength compared to control concrete specimens after 7 and 28 days of curing.

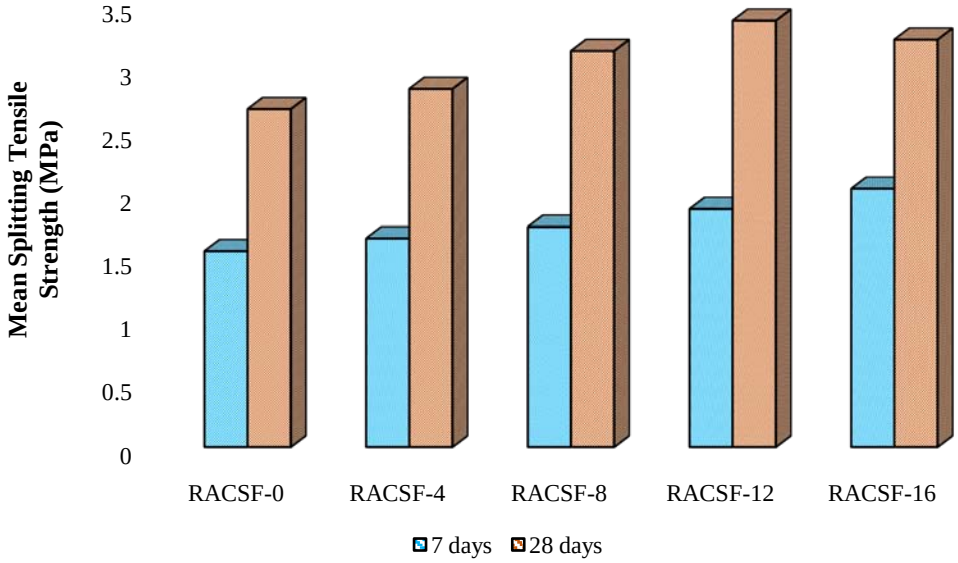

Figure 4: Splitting Tensile Strength Test Results of Racsf Mixes at 7 and 28 Days

Figure 6 shows that for silica fume concentrations nearby 12 percent, the gradual percentage change in splitting tensile strength of RACSF relative to the control specimen is greater (26.21%) at 28 days. The result is compared to a linear trend to verify the impact of silica fume replacement. Therefore, 12% is recommended to be optimal silica fume level. The lower value of the split tensile strength is caused by the decreased cohesive force between the aggregate surfaces and cement matrix, which enhances the lower binding tendency in the concrete mix. This conclusion is consistent with the findings of past tests [18].

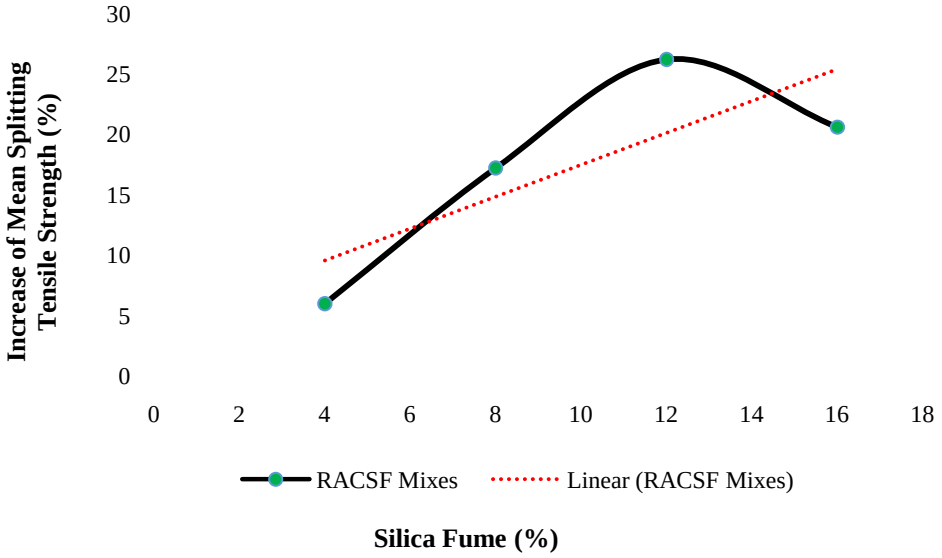

Figure 5: Percentage increase of splitting tensile strength 28 days

IV. CONCLUSIONS

Fifteen cube and fifteen cylindrical specimens with different replacement percentages of silica fume were put through compression and splitting tensile testing in this study. The following conclusions can be drawn based on the experimental findings:

1. Slump of concrete specimens decreased from 79 mm to 64 mm for the addition of silica fume.
2. For compressive strength, 12% addition of silica fume provided desired results. The maximum increase in concrete strength at 28 days was found to be 9.13% for RACSF-12 specimen compared to the reference specimen RACSF-0.
3. In case of splitting tensile strength, the percentage increase is much higher than compressive strength. The maximum increase in concrete strength at 28 days was found to be 26.21% for RACSF-12 specimen compared to the reference specimen RACSF-0. Thus 12% replacement of cement by silica fume is recommended as the optimal quantity for both compressive and splitting tensile strength.

Abbreviations

RAC	Recycled Aggregate Concrete
CDW	Construction and Demolition Waste
SCM	Supplementary Cementitious Materials
OPC	Ordinary Portland Cement
CH	Calcium Hydrate
CSH	Calcium Silicate Hydrate
SF	Silica Fume
ASR	Alkali Silica Reaction
NS	Nano Silica
W/C	Water to Cement Ratio

Conflicts of Interest

The authors declare no conflicts of interest.

REFERENCES

1. A. Akhtar and A. K. Sarmah, "Construction and demolition waste generation and properties of recycled aggregate concrete: A global perspective," *Journal of Cleaner Production*, vol. 186, pp. 262–281, 2018, doi: https://doi.org/10.1016/j.jclepro.2018.03.085
2. L. Butler, J. S. West, and S. L. Tighe, "The effect of recycled concrete aggregate properties on the bond strength between RCA concrete and steel reinforcement," *Cement and Concrete Research*, vol. 41, no. 10, pp. 1037–1049, 2011, doi: https://doi.org/10.1016/j.cemconres.2011.06.004.
3. B. Li *et al.*, "Effect of silica fume content on the mechanical strengths, compressive stress–strain behavior and microstructures of geopolymeric recycled aggregate concrete," *Construction and Building Materials*, vol. 384, p. 131417, Jun. 2023, doi: 10.1016/j.conbuildmat.2023.131417.
4. X. Song *et al.*, "Data-driven modeling for residual velocity of projectile penetrating reinforced concrete slabs," *Engineering Structures*, vol. 306, Mar. 2024, doi: 10.1016/j.engstruct.2024.117761.
5. S. Ahmad, K. O. Mohaisen, S. K. Adekunle, S. U. Al-Dulaijan, and M. Maslehuddin, "Influence of admixing natural pozzolan as partial replacement of cement and microsilica in UHPC mixtures," *Construction and Building Materials*, vol. 198, pp. 437–444, Feb. 2019, doi: 10.1016/j.conbuildmat.2018.11.260.
6. R. Sarkhani Benemaran, M. Esmaeili-Falak, and M. Kordlar, "Improvement of recycled aggregate concrete using glass fiber and silica fume," *Multiscale and Multidisciplinary Modeling, Experiments and Design*, vol. 7, pp. 1–20, Dec. 2023, doi: 10.1007/s41939-023-00313-2.
7. M. Shahab and N. Bashar, "Effect of silica fume on strength of recycled aggregate concrete," *International Journal of Research in Engineering and Innovation*, vol. 08, pp. 101–107, Jan. 2024, doi: 10.36037/IJREI.2024.8301.
8. M. R. Chowdhury and M. E. Hossain, "Green Building and Sustainable Development: Prospects and Challenges to Infrastructure Advancement of Bangladesh," 2021.
9. M. R. Chowdhury and S. A. Islam, "*Strategies to Make Buildings Green and Environment Friendly in Bangladesh: An Elementary Overview*".

10. M. R. Chowdhury and M. E. Kabir, "Applicability of Steel Fiber and Recycled Stone in Compressive Strength Development of M30 Concrete," 2023.
11. C09 Committee, *Standard Test Method for Slump of Hydraulic-Cement Concrete*. doi: 10.1520/C0143_C0143M.
12. R. Chowdhury, S. Islam, A. A. Swarna, and S. H. Noman, "Assessment of Galvanized Iron Fiber and Waste Tire Composite Concrete," vol. 11, no. 2.
13. K. Younis, R. Alzeebaree, A. Ismail, G. Khoshnaw, and T. Ibrahim, "Performance of Recycled Coarse Aggregate Concrete Incorporating Metakaolin," *IOP Conference Series: Earth and Environmental Science*, vol. 856, p. 012029, Sep. 2021, doi: 10.1088/1755-1315/856/1/012029.
14. A. Swarna, Md. Chowdhury, and Md. Noman, "Influence of Steel Fiber on Compressive Strength and Crack Pattern of Recycled Aggregate Concrete," *AJCE*, vol. 13, no. 2, pp. 61–67, Mar. 2025, doi: 10.11648/j.ajce.20251302.11.
15. Md. R. Chowdhury and D. Mondal, "Flexural Behavior of Recycled Aggregate Concrete Beam with Varying Dosage of Steel Fiber," *J. Eng. Res. Rep.*, vol. 26, no. 12, pp. 141–152, Dec. 2024, doi: 10.9734/jerr/2024/v26i121347.
16. Y. Tang, C. Zheng, F. Wanhui, N. Yumei, L. Cong, and C. Jieming, "Combined effects of nano-silica and silica fume on the mechanical behavior of recycled aggregate concrete," *Nanotechnology Reviews*, vol. 10, pp. 819–838, Aug. 2021, doi: 10.1515/ntrev-2021-0058.
17. R. Bajpai, K. Choudhary, A. Srivastava, K. S. Sangwan, and M. Singh, "Environmental Impact Assessment of Fly Ash and Silica Fume Based Geopolymer Concrete," *Journal of Cleaner Production*, vol. 254, p. 120147, May 2020, doi: 10.1016/j.jclepro.2020.120147.
18. F. Khademi and K. Behfarnia, "Evaluation of Concrete Compressive Strength using Artificial Neural Network and Multiple Linear Regression Models," *International Journal of Optimization in Civil Engineering*, vol. 6, pp. 423–432, Mar. 2016.